nature communications

Article

https://doi.org/10.1038/s41467-025-56002-w

# Increased SOAT2 expression in aged regulatory T cells is associated with altered cholesterol metabolism and reduced anti-tumor immunity

Received: 10 April 2024

Accepted: 7 January 2025

Published online: 13 January 2025

Check for updates

Mingjiong Zhang[1,7], Jiahua Cui[2,7], Haoyan Chen[1,7], Yifan Cheng[1,7], Qiaoyu Chen[3], Feng Zong[1], Xiao Lu[4], Lang Qin[5], Yu Han[1], Xingwang Kuai[6], Yuxing Zhang[1], Minjie Chu[2] ✉, Shuangshuang Wu[1] ✉ & Jianqing Wu[1] ✉

Immune functions decline with aging, leading to increased susceptibility to various diseases including tumors. Exploring aging-related molecular targets in elderly patients with cancer is thus highly sought after. Here we find that an ER transmembrane enzyme, sterol O-acyltransferase 2 (SOAT2), is overexpressed in regulatory T (Treg) cells from elderly patients with lung squamous cell carcinoma (LSCC), while radiomics analysis of LSCC patients associates increased SOAT2 expression with reduced immune infiltration and poor prognosis. Mechanically, ex vivo human and mouse Treg cell data and in vivo mouse tumor models suggest that SOAT2 overexpression in Treg cells promotes cholesterol metabolism by activating the SREBP2-HMGCR-GGPP pathway, leading to enhanced Treg suppresser functions but reduced $CD8^+$ T cell proliferation, migration, homeostasis and anti-tumor immunity. Our study thus identifies a potential mechanism responsible for altered Treg function in the context of immune aging, and also implicates SOAT2 as a potential target for tumor immunotherapy.

According to the latest global cancer data released by the International Agency for Research on Cancer (IARC), there were 19.29 million new cancer cases and 9.96 million deaths worldwide in 2021[1]. Among them, new cases of breast cancer reached 2.26 million, surpassing the 2.2 million cases of lung cancer, becoming the largest cancer globally. However, among males over 40 years old and females over 60 years old, lung cancer causes far more deaths than breast cancer, prostate cancer, colorectal cancer, and leukemia combined, making it the leading cancer that threatens the health of the elderly[2]. The incidence of lung squamous cell carcinoma (LSCC) is higher among the elderly and gradually increases with age. Nearly half of the patients are over 70 years old when diagnosed. Furthermore, the median survival of elderly LSCC patients is approximately 30% shorter than that of patients with other non-small cell lung cancer (NSCLC) subtypes[3]. Therefore, exploring the molecular mechanisms that influence the progression of elderly LSCC and finding specific therapeutic targets to improve the prognosis of elderly patients are of great significance.

[1]Jiangsu Provincial Key Laboratory of Geriatrics, Department of Geriatrics, The First Affiliated Hospital of Nanjing Medical University, Nanjing, China. [2]Department of Epidemiology, School of Public Health, Nantong University, Nantong, China. [3]Centre for Assisted Reproduction, Shanghai First Maternity and Infant Hospital, Tongji University School of Medicine, Shanghai, China. [4]Changshu Hospital Affiliated to Soochow University, Changshu No.1 People's Hospital, Changshu, China. [5]Department of Radiology, The First Affiliated Hospital of Nanjing Medical University, Nanjing, China. [6]Department of Pathology, Medical School, Nantong University, Nantong, China. [7]These authors contributed equally: Mingjiong Zhang, Jiahua Cui, Haoyan Chen, Yifan Cheng. ✉e-mail: chuminjie@ntu.edu.cn; polariswu7632@njmu.edu.cn; jwuny@njmu.edu.cn

The immune system identifies and eliminates aging and cancerous cells in the body, playing an important role in immune surveillance and maintaining the stability of the body's internal environment[4,5]. It is well recognized that the declined immune system function is one of the main characteristics of organism aging, which results in the occurrence of many aging-related diseases, such as tumors, autoimmune diseases, degenerative diseases of the central nervous system, and infections[5]. In addition, there are certain similarities in the mechanisms of aging and tumorigenesis. Growing evidence shows that alterations in the genome and epigenome, driven by similar mechanisms, are found in both aged cells and cancer cells[6]. Furthermore, nuclear cGAS can mediate the repression of L1 retrotransposition in both senescent and cancer cells induced by DNA damage agents[7]. Therefore, understating the causative relationships between tumor pathogenesis and aging is critical for the development of effective therapeutic strategies for tumor treatment in the elderly cancer patients.

Increasing evidence suggests that the enhanced immune function of regulatory T (Treg) cells is considered the culprit for poor prognosis in the elderly cancer population[8]. Treg cells rely on fatty acid oxidation and oxidative phosphorylation for survival, and promote proliferation, differentiation, and inhibitory function through glycolysis[9]. In addition, intracellular glycolipid metabolites affect the transcriptional program and functional plasticity of Treg cells by regulating the expression of FOXP3. Furthermore, mTORC1 promotes metabolic reprogramming of Treg cells in vivo, leading to increasing lipogenesis and cholesterol biosynthesis dependent on the mevalonate pathway, to support Treg cell proliferation and function[10]. The proportion of elderly individuals with disturbed glycolipid metabolism is much higher than that of young people. Exploring the functional changes of Treg cells after abnormal glycolipid metabolism may provide new clues for the treatment of elderly cancer patients.

Sterol O-acyltransferase 2 (SOAT2) is an endoplasmic reticulum (ER) transmembrane enzyme that converts cholesterol and fatty acids into cholesterol esters (CE) stored in cytoplasmic droplets, protecting cells from the toxicity of free cholesterol. The expression of SOAT2 in human leukocytes and monocytes regulates the differentiation and functional maintenance of immune cells. In addition, studies have shown that inhibiting the enzymatic activity of SOAT2 can suppress the proliferation of T cells[11,12]. However, the underlying mechanism of SOAT2-medicated regulation of Treg cells remains unclear.

In this study, we identify that SOAT2 gene is specifically overexpressed on Treg cells in elderly population. Using in vitro and vivo experiments, we observe SOAT2-expressed Treg cells induce effector T cell senescence by promoting cholesterol metabolism in Treg cells, and ultimately inhibiting anti-tumor immunity. SOAT2 overexpression in Treg cells promotes cholesterol metabolism in Treg cells by activating the SREBP2-HMGCR-GGPP pathway, leading to the induction of effector T cell senescence and suppression of anti-tumor immunity. These studies identify a novel mechanism responsible for the immune pathogenesis of tumors in elderly populations, demonstrating that SOAT2 could be a potential target for tumor immunotherapy.

## Results

### SOAT2 expression regulates immune infiltration and predicts clinical prognosis in elderly patients with lung squamous carcinoma

To evaluate the impact of immune signatures on the survivals of the elderly and young people with LSCC, a total of 459 samples were selected for analysis after excluding inappropriate survival times (Patients with follow-up durations shorter than 30 days or longer than 3650 days) in the TCGA-LSCC cohort. The overall survival of elderly patients was significantly lower than that of young patients (Fig. 1A; Supplementary Fig. 1A, B). Compared with young patients, there was no significant difference in the number of infiltrating immune cells and stromal cells in elderly patients (Fig. 1B, C). Furthermore, the survival of elderly patients was significantly lower than that of young patients in the presence of high immune cells and stromal cells in the tumor microenvironment (Fig. 1D, E). However, there was no difference in survival between elderly and young patients when both of the populations were with low infiltration of immune cells and stromal cells in the tumor microenvironment (Fig. 1F, G). Based on these findings, we speculate that the immune cell components in the tumor microenvironment of elderly patients may present a low immune response state leading to the reduced survival, compared with young patients.

We next screened 50 up-regulated and 133 down-regulated differentially expressed genes (DEGs) in elderly patients through an intersection calculation of immune and stromal cell infiltration differences within the tumor microenvironment (Fig. 1H). Kyoto Encyclopedia of Genes and Genomes (KEGG) pathway enrichment analysis showed that the 188 DEGs were participated in cholesterol metabolism, mTOR signaling, and Fc gamma R-mediated phagocytosis signaling pathways in older lung squamous carcinoma populations (Supplementary Fig. 1C). Simultaneously, multivariate Cox proportional hazards regression analysis revealed that 6/183 intersection DEGs (SUN3, ASF1B, STIM2, PCDHA13, SOAT2, GPR39) in the signatures were related to elderly patient's prognosis (Fig. 1I). Tumor Immune Estimation Resource (TIMER) further predicted the influences of 6 DEGs on immune cell infiltration, including B cells, $CD4^+$ T cells, $CD8^+$ T cells, macrophages, neutrophils, and dendritic cells. Among them, SOAT2 was identified to be correlated with $CD4^+$ T cell infiltration ($P < 0.01$) (Supplementary Fig. 1D). Consistent with these findings, the gene set enrichment analysis (GSEA: http://www.broadinstitute.org/gsea/index.jsp) and Gene Ontology (GO) enrichment confirmed that SOAT2 was positively related to T cell receptor signaling pathway (Fig. 1J; Supplementary Fig. 1E). Furthermore, GTEx data showed that the expression level of SOAT2 in the blood and spleens was increased with age (Fig. 1K, L; Supplementary Fig. 1F). In addition, the expression level of SOAT2 in elderly populations is significantly higher than that of young populations based on the data in the cohort of GSE62627 (Fig. 1M). Elevated SOAT2 expression may be associated with aging, which subsequently leads to poor prognosis in elderly LSCC patients. These data collectively support the notion that SOAT2 expression is involved in immune infiltration regulation that predicts clinical prognosis in elderly LSCC populations.

### Radiomic features associated with elevated SOAT2 expression predict poor prognosis in elderly LSCC patients

To investigate the functional role of SOAT2 in the impact of prognosis in elderly LSCC patients, we performed radiomics analysis with the computer-aided diagnosis technology and artificial intelligence algorithms. We obtained radiomics data of LSCC patients from the TCIA and TCGA databases to screen imaging features with prognostic value. In addition, 46 LSCC patients from The First Affiliated Hospital of Nanjing Medical University were collected and the imaging characteristics of SOAT2 differential expression were further analyzed. The study design was divided into three main stages (Fig. 2).

Stage 1 (Fig. 2A): We utilized the pyradiomics to extract 1714 radiomic features from 143 LSCC patients in TCIA, including morphological features (quantify the size and sphericity of the region of interest (ROI)), first-order histogram features (characterize the statistical properties of image intensity values), second-order histogram features (the gray-level co-occurrence matrix (GLCM), gray-level run-length matrix (GLRLM), gray-level size zone matrix (GLSZM), and neighborhood gray-tone difference matrix (NGTDM)). The consistency of 1714 radiomic features was also evaluated through the Intraclass Correlation Coefficient (ICC) analysis and standardized. Cluster analysis was performed on the standardized 1714 features, and the differential features with $P < 0.05$ were screened out

https://doi.org/10.1038/s41467-025-56002-w

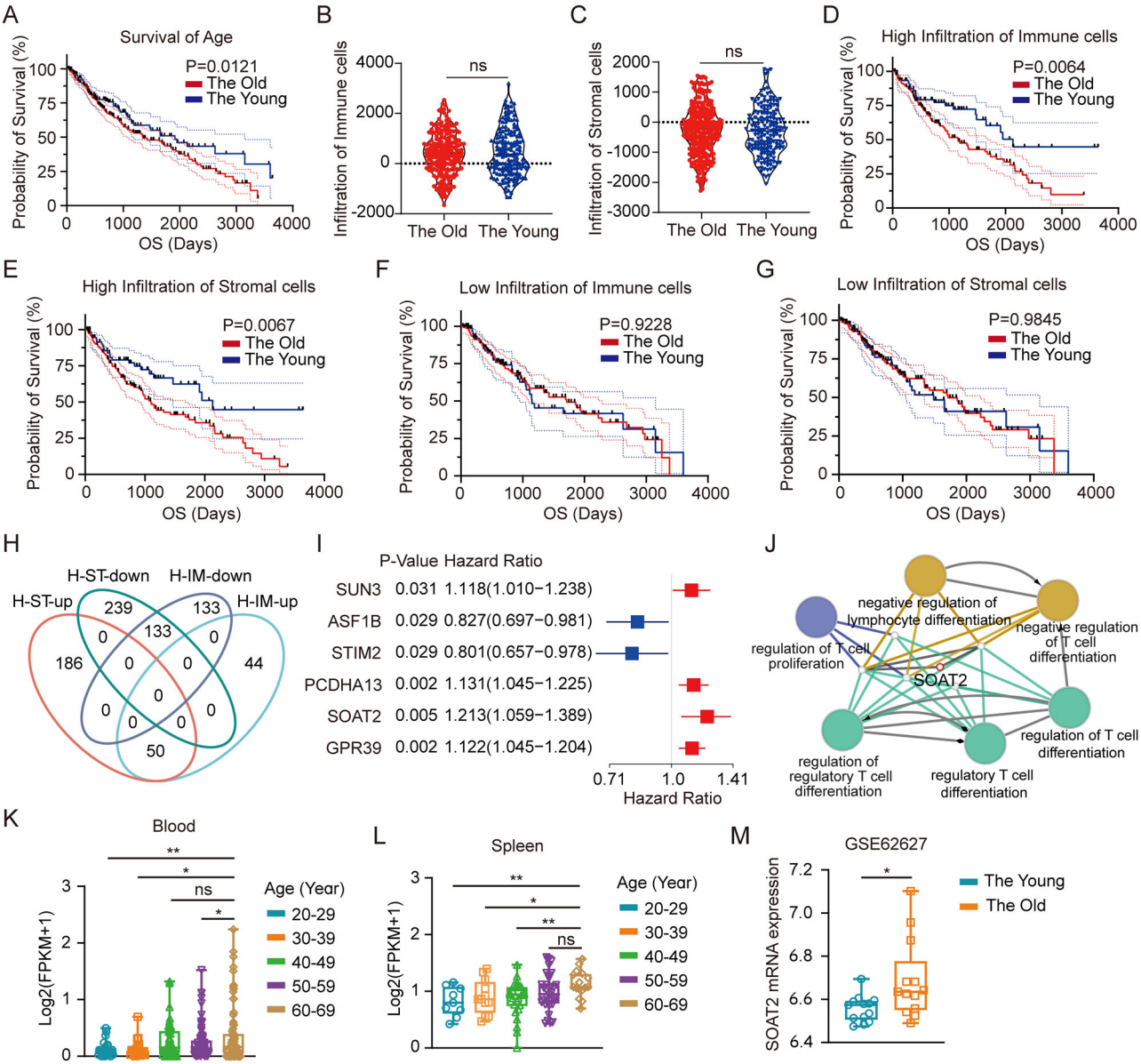


**Fig. 1 | SOAT2 involved in immune infiltration predicts poor prognosis in elderly patients with lung squamous carcinoma. A** Kaplan-Meier survival curves of LSCC patients grouped by age (The Old ≥ 65-year-old, $n = 293$; The Young <65-year-old, $n = 166$) in TCGA-LSCC cohort. **B**, **C** The infiltration of immune (**B**) and stromal (**C**) cells in the old and young populations. **D**, **E** Kaplan–Meier curves depicted Overall Survival in the old and young populations with high infiltration of immune (The Old: $n = 149$, The Young: $n = 80$) (**D**) and stromal (The Old: $n = 151$, The Young: $n = 78$) (**E**) cells. **F**, **G** Kaplan–Meier curves depicted Overall Survival in the old and young populations with low infiltration of immune (The Old: $n = 144$, The Young: $n = 86$) (**D**) and stromal (The Old: $n = 142$, The Young: $n = 88$) cells. **H** Venn diagram for screening differentially expressed genes in elderly patients based on tumor microenvironment immune and stromal cell infiltration differences. **I** Cox proportional hazards regression analysis showed 6 differentially expressed genes were related to elderly LSCC patient's prognosis ($n = 459$). **J** The gene set enrichment analysis indicated SOAT2 related signaling network. **K**, **L** The relative mRNA expression of SOAT2 was interrogated in the blood (**K**, Age 20–29: $n = 29$, 30–39: $n = 19$, 40–49: $n = 48$, 50–59: $n = 81$, 60–69: $n = 78$) and spleens (L, Age 20–29: $n = 9$, 30–39: $n = 12$, 40–49: $n = 26$, 50–59: $n = 34$, 60–69: $n = 16$) with different age in GTEx data. **M** The mRNA expression of SOAT2 was interrogated in the old and young populations by GSE62627 database (The Young: $n = 13$, The Old: $n = 13$). Data represented means ± SD. Statistical difference was evaluated by unpaired two-tailed student's *t*-test (**B**, **C**, **M**), and one-way ANOVA test (**K**, **L**). Source data are provided as a Source Data file. (*$P$ value < 0.05; **$P$ < 0.01; ns no significance).

(1302 differential radiomic features) (Supplementary Fig. 2A, B). The Least absolute shrinkage and selection operator (LASSO) regression analysis was then performed on the 1302 differential imaging features with prognosis as the outcome, and 3 radiomic features were selected: original_glszm_HighGrayLevelZoneEmphasis (gray-level size zone matrix feature), wavelet-HHH_glrlm_LongRunHighGrayLevelEmphasis (gray-level run-length matrix feature), and square_glszm_SizeZoneNonUniformityNormalized (gray-level size zone matrix feature) (Supplementary Fig. 2C, D).

Stage 2 (Fig. 2B): We verified the prognostic value of the 3 radiomic features of 37 LSCC patient imaging data from the TCGA database (Supplementary Fig. 2E). Subsequently, TCIA and TCGA data were merged, and radiomics and clinical information were combined to construct a Radiomics Clinical Nomogram Model to analyze the predictive effect of 3 radiomics features on survivals of LSCC patients. The results showed that these three radiomics features were associated with poor prognosis in LSCC patients (Supplementary Fig. 2F–H).

https://doi.org/10.1038/s41467-025-56002-w

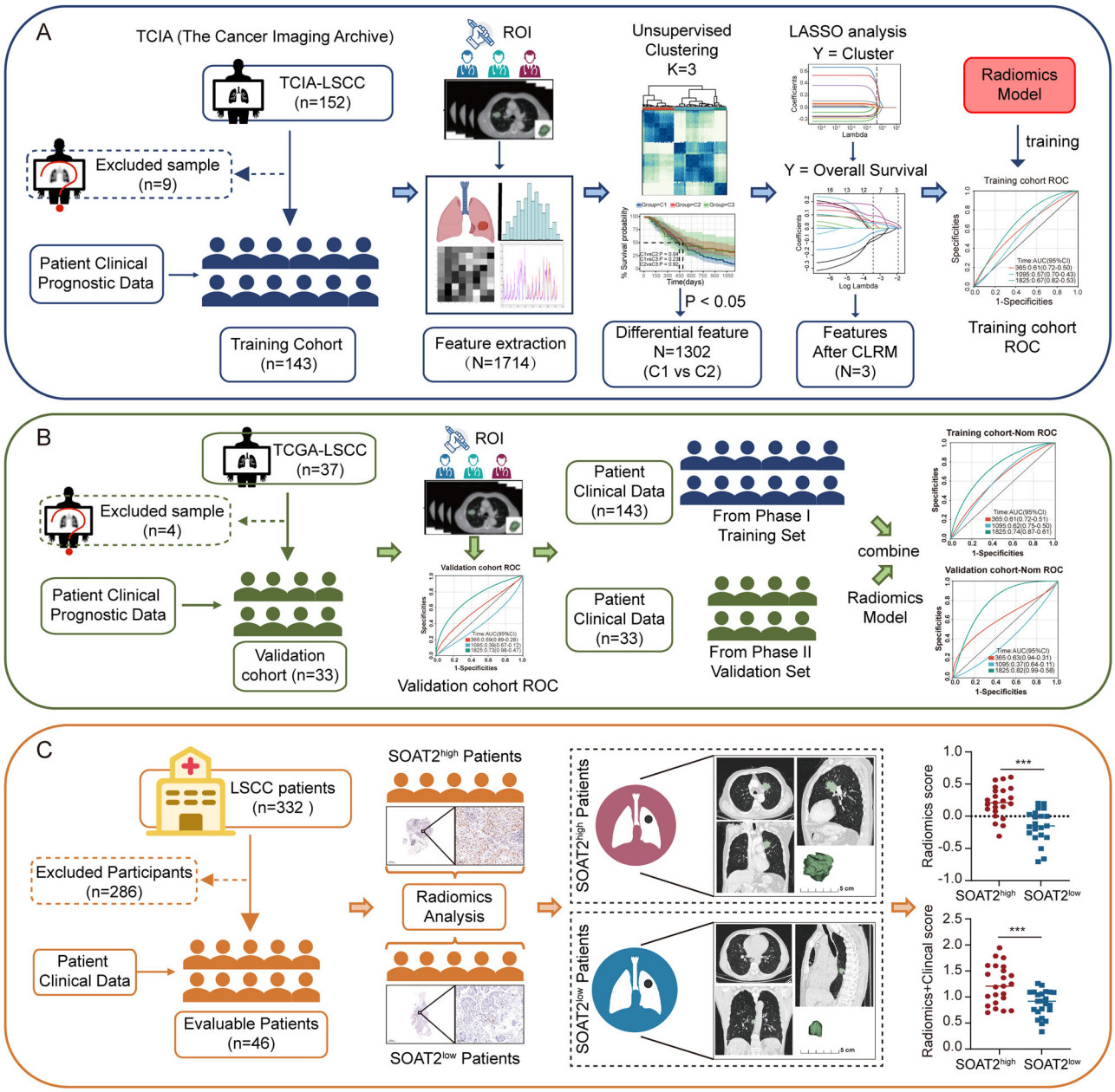


**Fig. 2 | Overview of the radiomics design. A** The training cohort: 143 Patients from the TCIA database were assigned to the training cohort, and 3 features with prognostic value were obtained. **B** The validation cohort: 33 Patients from the TCGA database were assigned to the validation cohort, and were evaluated whether the clinical features and risk score were independent of other radiomic features. **C** The analysis cohort: 46 patients from the First Affiliated Hospital of Nanjing Medical University were incorporated into the analysis. SOAT2 expression that predicts prognostic value in LSCC patients was validated in the independent cohort.

Stage 3 (Fig. 2C): We selected the LSCC patients over 65 years old from the First Affiliated Hospital of Nanjing Medical University in 2017 to 2019 for the analyses, excluding patients without preoperative imaging, histopathological testing, and missing follow-up. With the informed consent of the patients, 46 patients were included to analyze the radiomic features of SOAT2 differential expression. The Ki67 and SOAT2 staining of the 46 patients showed that SOAT2 promoted malignant tumor proliferation (Supplementary Fig. 3A, B). Furthermore, SOAT2 expression level was negatively correlated with the proportions of $CD4^+$ and $CD8^+$ cells, but positively correlated with Treg cells in the tumor microenvironment of LSCC patients (Supplementary Fig. 3C). These findings further reinforce the role of SOAT2 in modulating immune infiltration, thereby driving poor prognosis in elderly patients with LSCC. Moreover, we followed up with the post-operative patients included in the study and found that 11 out of 23 LSCC patients with high expression of SOAT2 developed tumor metastases, whereas only 4 out of 23 LSCC patients with low expression of SOAT2 had tumor metastasis (Supplementary Fig. 3D). The imaging reports further validated that the tumors with high expression of SOAT2 showed lobulated, spiculate, and highly infiltrated with surrounding lung tissue (Supplementary Fig. 3E). In addition, the radiomics analysis of 46 patients showed that high SOAT2 expression in tumor tissues predicted a worse prognosis in patients compared those of low SOAT2 expression (Supplementary Fig. 3F, G). These data collectively support the notion that SOAT2 expression is involved in immune infiltration regulation that predicts clinical prognosis in elderly LSCC

populations. Radiomics analysis showed that SOAT2 was associated with poor prognostic radiomics features of LSCC patients.

### High expression of SOAT2 promotes LSCC growth in old immunocompetent mice

To examine the function of SOAT2 in LSCC growth, we established a KLN-205 squamous cell carcinoma model in C57BL/6J mice (Fig. 3A). We purified PBMCs from young and old mice and detected the expression of SOAT2 by quantitative RT-PCR and Western Blotting analysis. We found that the expression of SOAT2 in PBMC of aged mice was significantly higher than that of young mice (Fig. 3B–D). We then selected the elderly mice with high and low expression of SOAT2, as well as young mice with low expression of SOAT2, and further evaluated the KLN-205 tumor growth with different ages and SOAT2 expression, respectively. As expected, we found that the KLN-205 tumor grew rapidly in aged mice compared with that of young mice. Furthermore, high expression of SOAT2 promoted tumor growth in aged mice (Fig. 3E–G). The Ki67 and SOAT2 staining of tumor tissues showed consistent results as shown with tumor growth (Fig. 3H–J). These data demonstrated that SOAT2 promotes LSCC growth in aged immunocompetent mice.

**Fig. 3 | SOAT2 promotes LSCC growth in old immunocompetent mice.** **A** Schematic design for screening the old mice with SOAT2$^{high}$ or SOAT2$^{low}$, and the young mice with SOAT2$^{low}$ (Created in BioRender. Major, Z. (2023) https://BioRender.com/l79u279). **B** The mRNA expression of SOAT2 in the young and old mice PBMCs was monitored by quantitative RT-PCR using gene-specific primers and probes ($n = 20$). **C**, **D** The protein expression of SOAT2 in the young and old mice PBMCs was monitored by western blotting analysis (**C**); quantitation of SOAT2 protein concentrations was shown ($n = 20$) (**D**). **E**–**G** The KLN-205 cells allograft-bearing model ($n = 5$). The tumor growth curves (**E**), representative images of subcutaneous tumors (**F**), and tumor weight (**G**) in indicated groups. **H** Representative immunohistochemical staining of ki67, SOAT2, FOXP3, and CD8 in the tumor nodules in indicated groups. scale bars: 2000 and 50 μm. **I**, **J** quantitation of ki67 (**I**); the correlation of SOAT2 with ki67 expression was shown ($n = 5$) (**J**). **K**–**M** Quantitation of FOXP3 integratedoption density (IntDen) and FOXP3-positive cells (**K**); the correlation of FOXP3-IntD and FOXP3-positive cells with SOAT2 expression were shown ($n = 5$) (**L**, **M**). **N**, **O** Quantitation of FOXP3 average optical density (AOD) (**N**); the correlation of FOXP3-AOD with SOAT2 expression was shown ($n = 5$) (**O**). **P**–**R** Quantitation of CD8-IntDen and FOXP3-positive cells (**P**); the correlation of CD8-IntD and CD8-positive cells with SOAT2 expression were shown ($n = 5$) (**Q**, **R**). **S**, **T** Quantitation of CD8 average optical density (AOD) (S); the correlation of FOXP3-AOD with SOAT2 expression were shown ($n = 5$) (T). Data represented means ± SD. Statistical difference was evaluated by unpaired two-tailed student's *t*-test (**B**, **D**), and one-way ANOVA test (**E**, **G**, **I**, **K**, **N**, **P**, **S**). Source data are provided as a Source Data file. (**$P < 0.01$; ***$P < 0.001$; ns no significance).

## SOAT2 is specifically expressed in Tregs of lung cancer elder patients

To explore whether SOAT2 regulates effector T or Treg cell infiltration in the tumor microenvironment, we performed CD8$^+$ and FOXP3$^+$ staining assay and observed an increase in FOXP3-positive cells within the tumor microenvironment (TME) in SOAT2$^{high}$ elder mice (Fig. 3K–M). However, upon analyzing the extracted FOXP3-positive cells, we found that FOXP3 expression decreased in SOAT2$^{high}$ elder mice (Fig. 3N, O). The expression of SOAT2 was inversely correlated with CD8$^+$ T cell infiltration (Fig. 3P–T). Increased FOXP3-positive cells suggested that SOAT2 may specifically regulate Treg cells within the tumor.

To further clarify the distribution of SOAT2 across diverse lymphocyte subtypes in aged mice, we separated CD4$^+$CD25$^+$, CD4$^+$CD25$^-$ and CD4$^-$lymphocyte subsets from tumor tissues and spleens in aged and young mice by magnetic bead sorting (Fig. 4A). We found that FOXP3, ICOS, GITR, CTLA-4, PD-1 is specifically overexpressed in CD4$^+$CD25$^+$ cells in tumor tissues and spleens from the tumor-bearing aged mice using western blotting analyses (Fig. 4B, C). Meanwhile, SOAT2 expression was consistent with that of FOXP3, CTLA-4, PD-1, ICOS, and GITR, suggesting its specific expression on Tregs (Fig. 4B, C). These results were further confirmed through the Flow Cytometry analyses (Fig. 4D–G). Meanwhile, we extracted CD4$^+$CD25$^+$, CD4$^+$CD25$^-$, and CD4$^-$ T lymphocytes from the blood of 30 elderly and young LSCC patients, and analyzed the expression of SOAT2 by RT-PCR and Western Blotting assay (Fig. 4H). The results showed that SOAT2 was predominantly expressed in Treg cells in elderly patients (Fig. 4I, J). Collectively, these data suggest that SOAT2 specifically expresses in Treg cells in aged LSCC individuals.

## SOAT2 enhances survival and chemotaxis but decreases proliferation and stability of Treg cells

The accumulation of Treg cells in the tumor microenvironment provides the foundation for their immune regulatory functions, which are governed by processes such as apoptosis, chemotaxis, proliferation, and cellular stability[13,14]. To examine the function of SOAT2 in regulating Treg cells, we established stable Treg cell lines with SOAT2 overexpression or knockdown (primary murine and human Treg cells). The overexpression and knockdown efficiencies of SOAT2 in Treg cells were confirmed by quantitative RT-PCR and Western Blotting assay (Supplementary Fig. 4A–D). We found that upregulation of SOAT2 in Treg cells significantly inhibited the proliferation of human Treg cells using the ki67 staining analysis. In contrast, suppression of the expression of SOAT2 by SOAT2 inhibitor Pyripyropene A promoted Treg cell proliferation (Fig. 5A, B). Similar results were observed in murine Treg cells, SOAT2-overexpression in Treg cells inhibited the Treg cell proliferation capacity, whereas, knockdown of SOAT2 promoted murine Treg cell proliferation (Fig. 5C, D). In addition, overexpression of SOAT2 in Treg cells attenuated $H_2O_2$-induced cell apoptosis, while knockdown of SOAT2 in Treg cells led to an increase in apoptosis upon $H_2O_2$ treatment (Fig. 5E, F; Supplementary Fig. 4E).

To explore the effect of SOAT2 on the chemotaxis of Treg cells, we established an indirect culture system of Treg cells and mouse-derived KLN-205 cells or human-derived H226 cells, respectively. We found that SOAT2-overexpression enhanced the chemotactic ability of Treg cells mediated by tumor cells, while the chemotactic ability of Treg cells was attenuated by SOAT2 knockdown in Treg cells (Fig. 5G, H). FOXP3 expression has been proven to be critical for Treg cell stability. The Flow Cytometry analysis showed that high expression of SOAT2 (SOAT2$^{high}$) in Treg cells inhibited the expression of FOXP3 in young individuals and SOAT2$^{low}$ restored FOXP3 expression in elderly individuals (Fig. 5I, J). In addition, SOAT2 over-expression in naïve T cells significantly decreased the frequency of Treg cell polarization after culture with Treg differentiation state for 72 h (Fig. 5K). These results indicate that SOAT2 expression in Treg cells enhances the survival and chemotaxis of Treg cells but decreases the proliferation and stability of Treg cells.

## SOAT2 promotes tumor growth through Treg-mediated immunosuppression

Treg cells promote tumor malignant progression mainly by inhibiting the proliferation of CD8$^+$ effector T cells (Teffs)[15]. To investigate the inhibitory effect of SOAT2$^{high}$ Treg cells on Teffs, we first generated tumor-reactive T cells by co-culture of human/murine PBMCs with lung squamous carcinoma cells (H226 or KLN-205 cells, respectively) according to previous reports (Supplementary Fig. 5A)[16,17]. We purified Teffs from tumor-reactive CD8$^+$ T cells with predominantly IFN-γ production and CD107a expression (Supplementary Fig. 5B, C). These cells specifically express MHC (Supplementary Fig. 5D–F), granzyme B (Supplementary Fig. 5G) and perforin (Supplementary Fig. 5H), confirming the successful purification of Teff cells. Then, the proliferative response of CFSE-labelled Teffs was measured by Flow Cytometry assay and confirmed that Treg cells strongly suppressed Teffs proliferation (Fig. 6A–C). Meanwhile, we found that co-culture of Teffs with SOAT2$^{high}$ Treg cells at a 0.2:1 ratio resulted in the strong suppression of Teff proliferation, while the suppressive activity of SOAT2$^{low}$ Treg cells on Teff proliferation was partially impaired based on the CFSE-labeling assays (Fig. 6A–C). As shown in Fig. 6D–F, co-culture with SOAT2$^{high}$ Treg cells inhibits the release of granzyme B and perforin from Teffs, while the suppressive activity was partially reversed after Pyripyropene A treatment using the ELISPOT assays. In addition, compared to co-culture with SOAT2$^{high}$ Tregs, co-culturing with SOAT2$^{Low}$ Tregs induces a greater release of granzyme B and perforin from Teffs (Fig. 6G–I). The ELISA assay further verified that the expression of SOAT2 in Treg cells has an immunosuppressive effect on Teff cells (Fig. 6J, K).

Subsequently, we analyzed the effect of Treg-mediated immunosuppression on tumor proliferation. We isolated Teffs that co-cultured with SOAT2$^{high}$ or SOAT2$^{low}$ Treg cells and measured its cytotoxicity to tumor cells. LDH release assay showed that compared

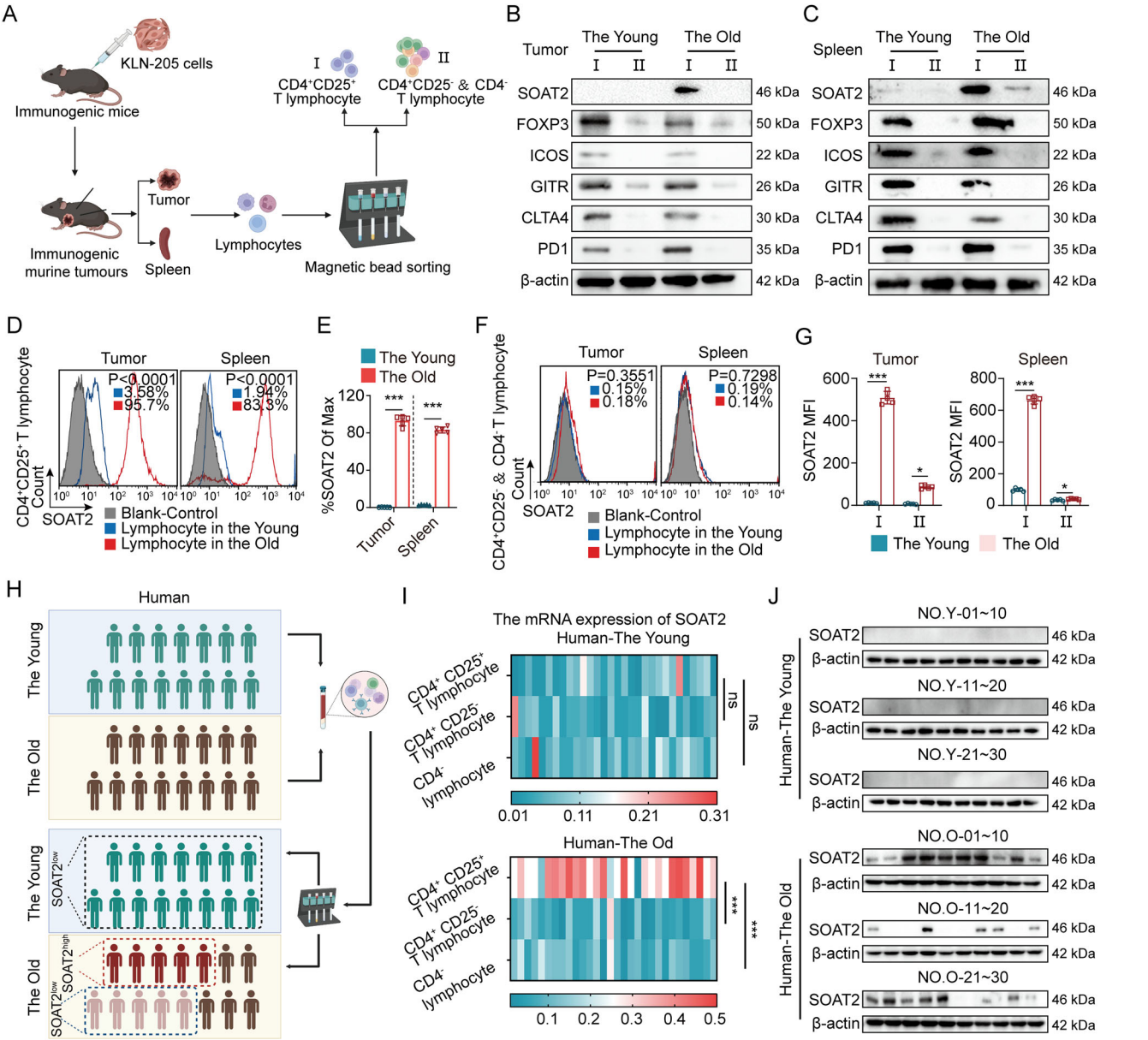


**Fig. 4 | SOAT2 specifically expresses in Treg cells in aged individuals. A** Diagram of murine $CD4^+CD25^+$, $CD4^+CD25^-$ T or $CD4^-$ lymphocytes isolated by magnetic bead sorting from LSCC tumor tissue and spleen samples (Created in BioRender. Major, Z. (2024) https://BioRender.com/u18t594). **B**, **C** The proteins extracted from tumor (**B**) and spleen (**C**) Lymphocyte subsets in indicated groups were assessed by Western blotting analysis. The experiment was repeated 3 times independently with similar results. **D**, **E** The SOAT2 expression was assessed in tumor and spleen $CD4^+CD25^+$ T lymphocytes by flow cytometry assay (**D**); quantitation of SOAT2 expression was shown ($n = 5$) (**E**). **F**, **G** The SOAT2 expression was assessed in tumor and spleen $CD4^+CD25^-$&$CD4^-$ T lymphocytes by flow cytometry assay (**F**); quantitation of SOAT2 expression was shown ($n = 5$) (**G**). **H** Diagram of human $CD4^+CD25^+$ T lymphocytes, $CD4^+CD25^-$ T or $CD4^-$ lymphocytes isolated by magnetic bead sorting from blood samples (Created in BioRender. Major, Z. (2024) https://BioRender.com/w00f660). **I**, **J** The mRNA and protein expression of SOAT2 in indicated groups were detected by quantitative RT-PCR (**I**) and Western blotting (**J**, The experiment was repeated 3 times independently with similar results) analysis. Data represented means ± SD. Statistical difference was evaluated by unpaired two-tailed student's *t*-test (**E**, **G**), and one-way ANOVA test (**I**). Source data are provided as a Source Data file. (*$P < 0.05$; ***$P < 0.001$; ns no significance).

with the control, tumor cells co-cultured with $SOAT2^{low}$ Treg-treated Teffs had more tumor cell death; whereas, Teffs treated with $SOAT2^{high}$ Treg cells had a weak cytotoxicity to tumor cells (Fig. 6L, M). These data suggest that SOAT2 promotes tumor growth through Treg-mediated immunosuppression on effector T cells.

### SOAT2-expressed Treg cells induce Teff cell senescence via competitive cholesterol metabolism of Treg cells

The accumulated tumor-infiltrating Treg cells exert the immunosuppressive function mainly by promoting cellular apoptosis, exhaustion, and senescence in Teffs, which is associated with poor clinical outcomes in aged patients[18–21]. We found that co-culture with $SOAT2^{high}$ Treg cells did not induce the apoptosis of Teffs (Supplementary Fig. 6A, B). Western Blotting assay further confirmed this finding (Supplementary Fig. 6C). However, after co-culture with $SOAT2^{high}$ Treg cells, Teffs showed DNA damage and repair characteristics (Supplementary Fig. 6D–G). These results suggest that overexpression of SOAT2 in Treg cells may promote senescence or exhaustion of Teffs, thereby exerting immunosuppression. Flow Cytometry assays confirmed that co-culture with $SOAT2^{high}$ Treg cells induced Teffs

https://doi.org/10.1038/s41467-025-56002-w

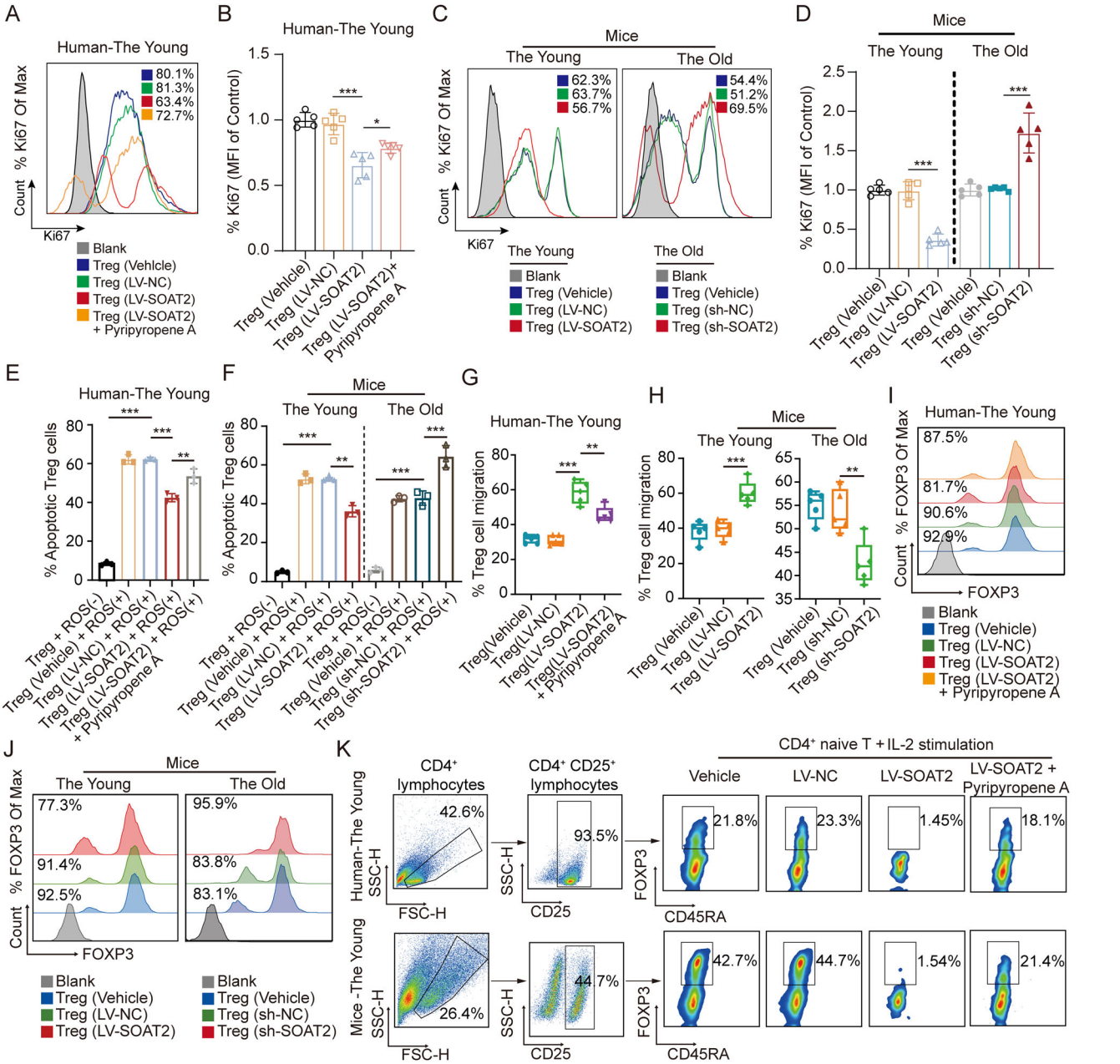


**Fig. 5 | SOAT2 enhances survival and chemotaxis but decreases proliferation and stability of Treg cells. A–D** Ki-67 staining in indicated groups was analyzed by flow cytometry to measure lymphocyte proliferation (**A**, **C**); quantitation of Ki67 of Max (%) was shown ($n = 5$) (**B**, **D**). **E**, **F** The apoptotic Treg cells in indicated groups were analyzed by flow cytometry with 7-AAD and PE-Annexin V staining; the percentage of apoptotic Treg cells in indicated groups were shown ($n = 3$). **G**, **H** The migration of Treg cells in indicated groups were detected by transwell assays ($n = 5$). **I**, **J** FOXP3 staining in indicated groups was analyzed by flow cytometry to measure Treg cells stability. **K** The differentiation ability of naive $CD4^+$ T cells to $CD4^+CD25^+FOXP3^+$ T lymphocytes sorted in indicated groups under Treg polarizing conditions was detected by flow cytometry assay. Data represented means ± SD. Statistical difference was evaluated by one-way ANOVA test (**B**, **D**, **E**, **F**, **G**, **H**). Source data are provided as a Source Data file. (*$P < 0.05$; **$P < 0.01$; ***$P < 0.001$).

senescence but did not affect Teffs exhaustion (Supplementary Fig. 6H–O).

To investigate whether $SOAT2^{high}$ Treg cells induce senescence in Teff cells, we performed senescence-associated β-galactosidase staining of Teffs after co-culture with Treg cells that transduced with lentiviral-based SOAT2 or shRNA against SOAT2. The results showed that the senescent cell populations were much higher in Teffs that co-cultured with $SOAT2^{high}$ Treg cells in the young group, while induction of Teff cell senescence was severely blunted after SOAT2 knockdown in Treg cells from the old group (Fig. 7A–C). The results from the analysis of cellular senescence-associated molecules further indicate that the expression of P16, P21, and P53 were much higher in Teffs that co-cultured with $SOAT2^{high}$ Treg cells in the young group, while the expression was severely blunted after SOAT2 knockdown in Treg cells from the old group (Fig. 7D–F). Loss of CD27 and CD28 expression in Teffs is associated with senescence induction mediated by Treg cells. We also found that $SOAT2^{high}$ Treg cells aggravated the loss of CD27/CD28 expression in Teffs, while knockdown of SOAT2 in Treg cells partially reversed the loss of CD27/CD28 in Teffs (Fig. 7G–J). The finding was subsequently confirmed by detecting CD27 and CD28 double negative population in Teffs (Supplementary Fig. 7A–D). These results indicated that $SOAT2^{high}$ Treg cells potently induce Teff cell

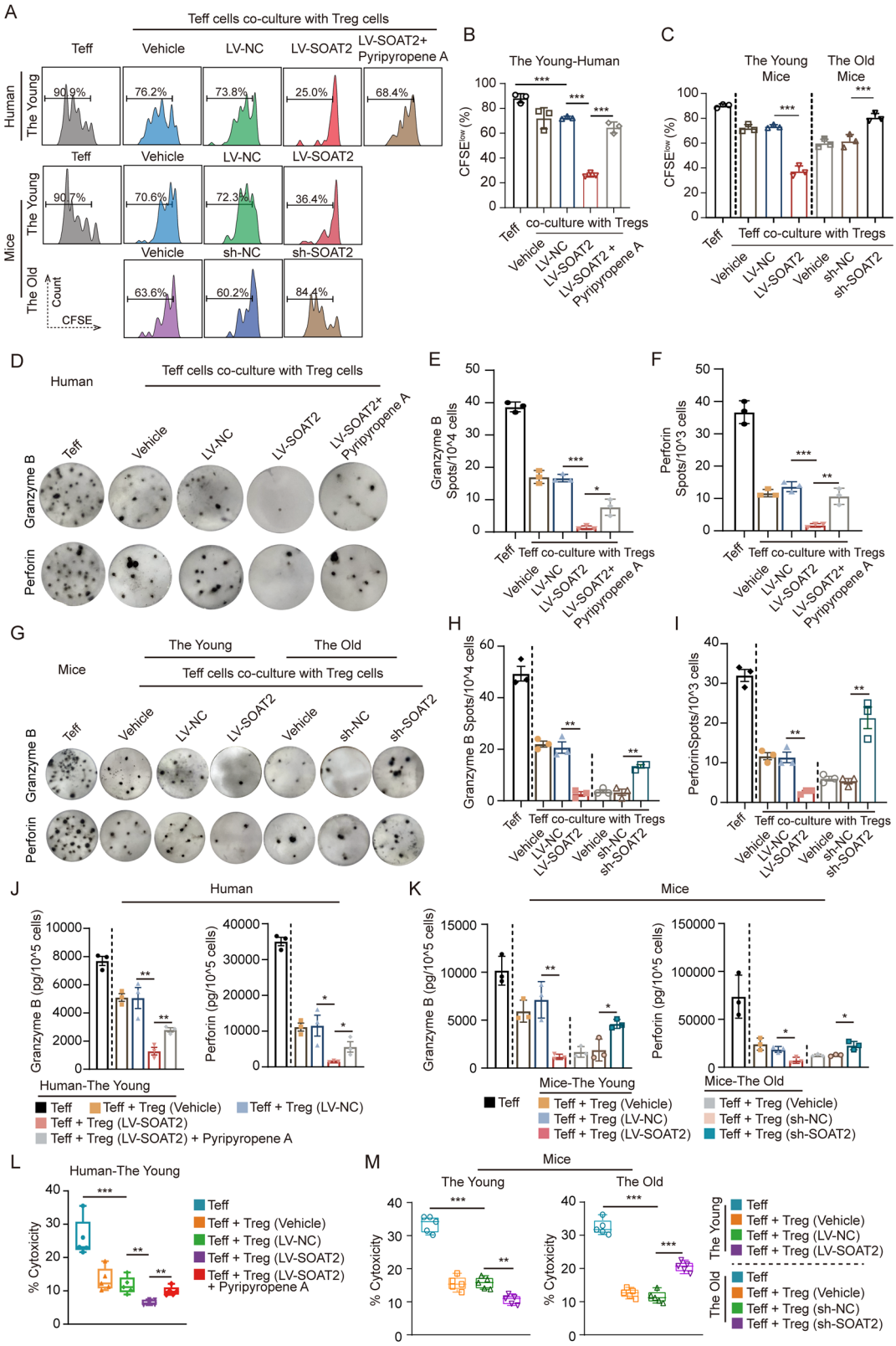


senescence. However, senescent Teff cells do not exhibit the senescence-associated secretory phenotype (Supplementary Fig. 7E).

It has been reported that Treg-mediated immune suppression is through the competition of cholesterol uptake and IL2 consumption with Teffs; and secreting immunosuppressive factors, including IL-10, TGF-β, and IL-35 etc. (Fig. 7K)[22–25]. SOAT2 did not affect IL-2 levels in the culture media and the release of IL10, IL35 and TGFβ in Treg cells (Supplementary Fig. 7F–M). Furthermore, overexpression of SOAT2 significantly increased cholesterol uptake by Treg cells, which was reversed by pyripyropene A (Fig. 7L, M). While knockdown of SOAT2 ($SOAT2^{Low}$) significantly decreased cholesterol uptake by Treg cells (Fig. 7M). The SOAT2 gene encodes for a cytosolic enzyme involved in the regulation of lipid metabolism and cholesterol metabolism, which in turn has an impact on cell function. Our bioinformatical analyses

**Fig. 6 | SOAT2 promotes tumor growth through Treg-mediated immunosuppression. A–C** Treg cells were co-cultured with CFSE-labeled $CD8^+$ T lymphocytes at a 0.2:1 ratio in indicated groups, and $CD8^+$ T lymphocytes proliferation expansion was detected by flow cytometry assay (**A**); quantitation of $CFSE^{Low}$ (%) was shown ($n = 3$) (**B**, **C**). **D–I** Treg cells were co-cultured with $CD8^+$ T lymphocytes at a 0.2:1 ratio in indicated groups, and the release of $CD8^+$ T lymphocytes for granzyme B and perforin were detected by ELISPOT assay (**D**, **G**); quantitation of granzyme B (**E**, **H**) and perforin (**F**, **I**) were shown (biological replicate, $n = 3$). **J**, **K** Treg cells were co-cultured with $CD8^+$ T lymphocytes at a 0.2:1 ratio in indicated groups, and the release of $CD8^+$ T lymphocytes for granzyme B and perforin were detected by ELISA assay; quantitation of granzyme B and perforin were shown ($n = 3$). **L**, **M** Treg cells were co-cultured with $CD8^+$ T lymphocytes at a 0.2:1 ratio in indicated groups, and Teff-mediated cytoxicity was determined by LDH release assay using a cytotoxicity detection kit ($n = 5$). Data represented means ± SD. Statistical difference was evaluated by one-way ANOVA test (**B**, **C**, **E**, **F**, **H**, **I**, **J**, **K**, **L**, **M**). Source data are provided as a Source Data file. ($^*P < 0.05$; $^{**}P < 0.01$; $^{***}P < 0.001$).

also indicated that SOAT2 was involved in regulation of cholesterol metabolism in Treg cells from the elderly LSCC patients (Supplementary Fig. 1C). To further explore the effect of SOAT2 on cholesterol metabolism, cholesterol transport and homeostasis in Treg cells, we detected the mRNA expression of related molecules by RT-PCR assay (Supplementary Fig. 8A). We found that compared with young individuals, Treg cells in elder individuals had higher gene expression of cholesterol metabolic enzyme (Supplementary Fig. 8B, C). However, no significant differences were detected in the LXR-related genes between the two groups (Supplementary Fig. 8D). We further confirmed that the total cholesterol and cholesteryl ester concentrations of Treg cells in elderly individuals were more than those in young individuals; whereas, the free cholesterol concentration of Treg cells in elderly individuals were less than those in young individuals (Supplementary Fig. 8E–G).

We then explored the regulatory effect of SOAT2 on cholesterol metabolism of Treg cells. As shown in Supplementary Fig. 8H–J, RT-PCR analysis showed that SOAT2-overexpression in Treg cells enhanced the expression of cholesterol synthase (Mvd), cholesterol regulatory factor binding protein (Srebf2), and cholesterol synthesis catalytic enzyme (Hmgcr), while the expression of Mvd, Srebf2, and Hmgcr were attenuated by SOAT2 knockdown in Treg cells. These results were subsequently confirmed by Western Blotting analysis (Supplementary Fig. 8K, L). In addition, cholesterol suppression by Methyl-β-cyclodextrin (MBCD) can promote Treg-induced Teff cell senescence in both human and mice. While addition of cholesterol metabolite 25-hydroxycholesterol (25-HC) can reverse $SOAT2^{high}$ Treg-induced Teff cell senescence in both human and mice (Fig. 7N–P). Collectively, these data suggest that SOAT2 expression in Treg cells can promote Teff cell senescence via competitive cholesterol uptake of Treg cells with Teff cells.

## SOAT2 promotes cholesterol metabolism in Treg cells by activating the SREBP2-HMGCR-GGPP pathway

The sterol-regulatory element binding proteins (SREBPs) are the main feedback regulation of intracellular cholesterol metabolism (Fig.8A). SREBP1 and SREBP2 promote activation of downstream HMGCR, and the activation of these transcription factors is mediated by S6 Phosphorylation[26]. To investigate the effect of SREBP2 on cholesterol metabolism in Treg cells, we employed well-defined SREBP2 agonist Methyl-β-cyclodextrin (MBCD) and SREBP2 inhibitor 25-hydroxycholesterol (25-HC), combined with SOAT2-overexpression or SOAT2-knockdown to regulate the cholesterol metabolism in Treg cells. ELISA assay showed that the decreased free cholesterol concentration in $SOAT2^{high}$ Treg cells could be upregulated by SREBP2 inhibitor 25-HC; and the increased free cholesterol concentration could be downregulated by SREBP2 agonist MBCD (Fig. 8B, C). In addition, the decreasing protein expression of FOXP3, and the increasing protein expression of CCR6, MCL1 and NRP1 in $SOAT2^{high}$ Treg cells could be reversed by SREBP2 inhibitor 25-HC; the opposite regulatory effect of FOXP3, CCR6, MCL1 and NRP1 in $SOAT2^{Low}$ Treg cells could be reversed by SREBP2 agonist MBCD (Fig. 8D, E).

We next used HMGCR metabolite GGPP, GGPP inhibitor Digeranyl bisphosphonate (DGBP), MBCD, and 25-HC to regulate relevant targets of the SREBP2 metabolic pathway and explored the changes in cholesterol metabolism in Treg cells. The results further confirmed the important role of SREBP2-HMGCR-GGPP pathway in regulating cholesterol metabolism in Treg cells (Fig. 8F, G). To verify the effect of SREBP2/HMGCR/GGPP signaling on Treg cell cholesterol metabolism in elderly LSCC patients, we detected the protein expression of the key molecules in SREBP2/HMGCR/GGPP signaling pathway using Western Blotting assays. We observed that the protein expression of HMGCR, Raptor, p-4EBP1, p-S6, Mcl-1, CCR6, and Nrp1 were increased, while Rictor, and FOXP3 were significantly decreased after over expression of SOAT2 in Treg cells. The alterations of key molecules in SREBP2/HMGCR/GGPP pathway regulated by SOAT2 in Treg cells were reversed by the GGPP inhibitor DGBP (Fig. 8H).

We next determined the effect of the SREBP2-HMGCR-GGPP signaling pathway in regulating Treg cell functions. The GGPP, DGBP MBCD and 25-HC were used to treat the Treg cells, and evaluated the cell proliferation, cytotoxic activity, apoptosis, chemotaxis, and polarization phenotypes, using Ki67 staining (Supplementary Fig. 9A), LDH assay (Supplementary Fig. 9B), propidium iodide (PI) apoptosis assay (Supplementary Fig. 9C–E), cell migration assay (Supplementary Fig. 9F, G), cell polarization experiment (Supplementary Fig. 9H–K), respectively. Overexpression of SOAT2 in Treg cells inhibited the proliferation cytotoxic activity, and polarization of Treg cells, but enhanced apoptosis resistance and the chemotaxis of Treg cells. The treatment of GGPP can further inhibit the proliferation, cytotoxic activity and polarization of Treg cells, but enhance apoptosis resistance and the chemotaxis of Treg cells. However, DGBP treatment yielded the opposite effects on Treg functions as shown in GGPP treatment.

Subsequently, we further verified the effect of the SREBP2-HMGCR-GGPP signaling pathway in Treg cell-mediated suppression on Teffs. Under co-culture of Treg cells and Teffs, we added the GGPP, DGBP MBCD, or 25-HC into the co-cultures, and then evaluated the proliferation, apoptosis, and cellular senescence phenotypes in Teffs, using Flow cytometry analysis (Supplementary Fig. 10A–E) and β-galactosidase staining (Supplementary Fig. 10F–H), respectively. Consistent to the previous results, we found that $SOAT2^{high}$ Treg cells inhibited the proliferation of Teff cells and promoted Teff cell senescence rather than apoptosis. The treatment of GGPP can further inhibit the proliferation of Teffs and promote Teff cell senescence. In contrast, DGBP treatment yielded the opposite phenotypes as shown in GGPP treatment.

To further elucidate the impact of cholesterol metabolism on tumor growth, we established a tumor-bearing mouse model using aged mice fed with a high-fat diet (Fig. 9A). The results showed that increasing doses of simvastatin corresponded with a progressive decrease in cholesterol levels in plasm in different groups of tumor-bearing mice, while SOAT2 expression remained comparable levels in Treg cells across the groups (Fig. 9B–D). Cholesterol inhibition significantly suppressed tumor growth in the mice. Notably, the high-dose simvastatin group (50 mg/kg) exhibited accelerated tumor growth compared to the medium-dose simvastatin group (25 mg/kg) (Fig. 9E–G). These findings suggest that in mice with elevated SOAT2 levels, a more potent reduction in cholesterol levels may enhance Treg function, whereas under conditions of sufficient cholesterol levels primarily affects tumor cells with minimal impact on Treg function and infiltration. In summary, SOAT2 expression promotes cholesterol

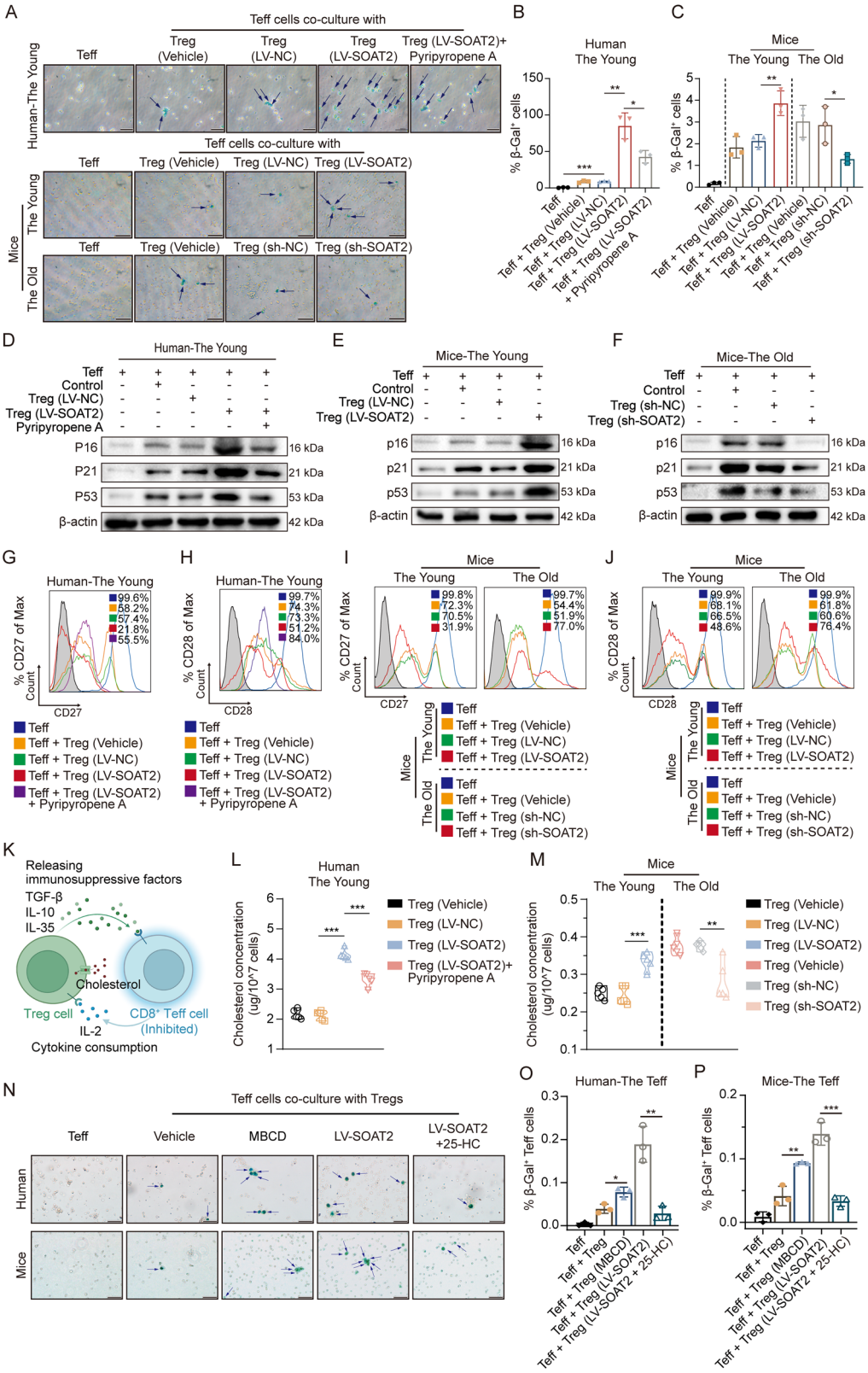


metabolism in Treg cells by activating the SREBP2-HMGCR-GGPP signaling pathway.

## Discussion

Lung squamous carcinoma is considered an aging-related disease accompanied by a remodeling process in the immune system, which is known as Immunosenescence[27]. Immunosenescence in elderly populations is characterized by immune dysfunction and inflammatory cytokines infiltration[28]. This demonstrates that the elderly populations received limited benefits from traditional chemotherapy, radiotherapy, and immunotherapies, which lead to a worse survival prognosis compared to the young individual[29,30]. Given that treatment options for elderly LSCC patients are limited, our work may provide a new immune target

**Fig. 7 | SOAT2 induces Teffs cellular senescence via competitive cholesterol metabolism of Treg cells. A–C** Representative images of Teffs stained for β-galactosidase (arrows) after co-cultured with Treg cells ($n = 3$) (**A**), scale bars: 50 μm; quantitation of β-galactosidase-positive Teffs were shown (**B**, **C**). **D–F** The protein expression of P16, P21, P53 in Teff cells in the young and old individuals were monitored by western blotting analysis in indicated groups. The experiment was repeated 3 times independently with similar results. **G–J**, Treg cells were co-cultured with $CD8^+$ T lymphocytes at a 0.2:1 ratio in indicated groups, and the expression of CD27 or CD28 in human Teffs (**G**, **H**) and murine Teffs (**I**, **J**) were detected by flow cytometric analysis ($n = 3$). **K** Schematic representation of Treg cells exerts immunosuppressive path on Teffs (Created in BioRender. Major, Z. (2024) https://BioRender.com/s68z662). **L**, **M** The content of cholesterol components were measured by the Cholesterol Assay Kit in indicated groups ($n = 5$). **N–P** Representative images of Teffs stained for β-galactosidase (arrows) after co-cultured with Treg cells (N), scale bars: 50 μm; quantitation of β-galactosidase-positive Teffs were shown ($n = 3$) (**O**, **P**). Data represented means ± SD. Statistical difference was evaluated by one-way ANOVA test (**B**, **C**, **L**, **M**, **O**, **P**). Source data are provided as a Source Data file. (*$P < 0.05$; **$P < 0.01$; ***$P < 0.001$).

and perspective for precise tumor treatment. Based on TCGA-LSCC cohort, we found that SOAT2 can be exploited as a therapeutic target in Treg cells evaluated by ESTIMATE algorithms. Both in vitro and vivo experiments supported the notion that aberrantly expression of SOAT2 in Treg cells in elderly individuals enhances the susceptibility to tumors by activating cholesterol metabolic pathways to regulate itself proliferation, migration, stability, and immunosuppression. Furthermore, the immunosuppression is dependent upon the SREBP2/HMGCR/GGPP signaling pathway in Treg cells.

Aging-associated immune dysfunction is considered to be highly correlated with tumorigenesis and evolution[5,31]. The immune system in aging is intricate and multifaceted, involving the reconstruction of adaptive immune function, which is thought to be closely related to the aging process[32,33]. Regulatory T cells are a specialized T cell subset involved in the immunosuppressive loop of immune remodeling process and promoting peripheral tolerance[34]. Regulatory T cells modulate antigen-presenting cells (APCs) via CTLA-4, thereby indirectly suppressing effector T cell function through mechanisms such as competitive blockade of the CD28 co-stimulatory signal, down-regulation of the co-stimulatory molecules CD80/CD86, and induction of immune-suppressive signaling. These mechanisms act synergistically to maintain an immunosuppressive milieu, which is of critical importance in the tumor microenvironment and chronic inflammation. In mammalian species, the accumulation of Treg cells in various organs and circulatory systems is widely observed during the aging progression[35]. Previous studies have revealed that the increased frequency of aging-related Treg cells is linked to the reinforced proliferative capacity, the enhanced survivability, or the lineage-specific differentiation[36,37]. Chougnet CA, et al. showed that Treg cells from aged mice exhibited superior anti-apoptotic capacity compared to those from young mice, and the differentiation capacity of $CD4^+CD25^+FOXP3^+$ T cells from naïve $CD4^+$ T cells were significantly reduced in aged mice[36]. This study demonstrates that SOAT2 is specifically expressed in Treg cells of elderly individuals compared to younger individuals. Overexpression of SOAT2 significantly extends Tregs survival while inhibiting their proliferation and differentiation. The reduced proliferative effect of $SOAT2^{high}$ Treg cells is to avoid undergoing multiple copies, which results in a generation of the oligoclonal Treg cells with function-weakening, thereby enhancing immunosuppressive effects and reducing age-dependent cell damage. In addition, overexpression of SOAT2 in Treg cells was correlated with reduced FOXP3 expression, and higher cellular instability. As shown in Fig. 4B, CTLA-4 is highly expressed in tumor-infiltrating Tregs from both young and aged mice, indicating that the APC-dependent immune suppressive function of Tregs is conserved across age groups. However, compared with young mice, the immune function of aged mice was further suppressed. These findings suggest that in aged mice, SOAT2 further suppresses immune function through an APC-independent mechanism.

Both in vivo and in vitro experiments showed that Treg cells with SOAT2 overexpression induce Teffs senescence by rapidly usurping the supply of its essential cholesterol, leading to the weak anti-tumor immunity of Teff in elderly LSCC patients. In the young mammalian immune system, the metabolism of Teffs depends on glycolipid metabolites, while Treg cells exhibit a high rate of lipid oxidation and suppression of glycolysis[38,39]. Moreover, when subjected to external stressors such as chronic inflammation[40], the lipid metabolism in Treg cells will shift towards enhanced glycolytic metabolism. Age-associated immunosenescence describes a reduction in adaptive immunity and an increase in release of various inflammatory mediators, shaping a metabolic environment[41]. In such conditions, augmented glycolipid metabolism contributes to Treg cell suppressive function in the tumor microenvironment, while modulation of cholesterol metabolism can reverse T cell functionality[42–45]. The study also confirms this conclusion.

SOAT2, an important member of the acyl coenzyme A family involved in cholesterol metabolism[46], is mainly distributed in the liver and intestines[47]. This study investigated that SOAT2 was scarcely expressed in Treg cells isolated from younger individuals but abundantly expressed in older individuals. Consistently, SOAT2 was barely expressed in non-Treg cells in young and older individuals. These findings suggested a possible link between acquired genetic alteration and age-induced immunity remodeling. In this study, we found that SOAT2 converts long-chain fatty acyl-CoA and free cholesterol into intracellular cholesteryl esters, thereby reducing free cholesterol[47,48]. As the primary sensor and regulator of cellular cholesterol levels, SREBP2 is activated once intracellular free cholesterol levels decrease[49]. The activated SREBP2 pathway increases HMGCR transcripts, thereby upregulating the mevalonate pathway[50]. Hu Zeng et al. found that Geranilgerarnyl pyrophosphate (GGPP), a metabolite in the mevalonate pathway, mediates the activation of mTORC1, while reducing mTORC2 activity to promote the function of Treg cells[10]. Here, we demonstrate that activation of the SOAT2-regulated mevalonate pathway mediates this metabolic reprogramming, which significantly promotes the regulation of critical functionally related proteins, including mSrebp2, Hmgcr, Raptor, p-4EBP1, p-S6, Mcl-1 and Nrp1. Similar to our results, Timilshina et al. showed that the LKB1-mediated mevalonate pathway is required for immunosuppression and stability of Treg cells[51]. Lim et al. found that the activity of SREBPs is upregulated in intratumoral Treg cells and enhances the functional specialization of Treg cells in tumors through lipid signaling[22]. Prado et al. demonstrated that preventing further activation of the mevalonate pathway by pitavastatin enhanced the suppressive function of Treg cells in vitro[52].

Metabolic alterations that may impact SOAT2 expression and are associated with aging include: (1) Purine degradation compounds: Elevated levels in elderly individuals are linked to changes in cellular and nucleic acid metabolism. (2) Complement peptides: Increased levels of these immune-related metabolites may correlate with heightened inflammatory responses during aging. (3) Ornithine: Higher concentrations of this urea cycle intermediate are observed in elderly individuals. (4) Polyunsaturated fatty acids (PUFAs): Increased levels in the elderly reflect alterations in lipid metabolism. (5) Cytochrome P450-related metabolites: Elevated levels of these compounds are involved in drug metabolism and the conversion of endogenous substances. (6) Uric acid: Elevated levels of this metabolite may be present in elderly individuals. (7) Phenylalanine: Increased levels of this amino acid in elderly individuals indicate modifications in metabolic pathways. These metabolic changes are

https://doi.org/10.1038/s41467-025-56002-w

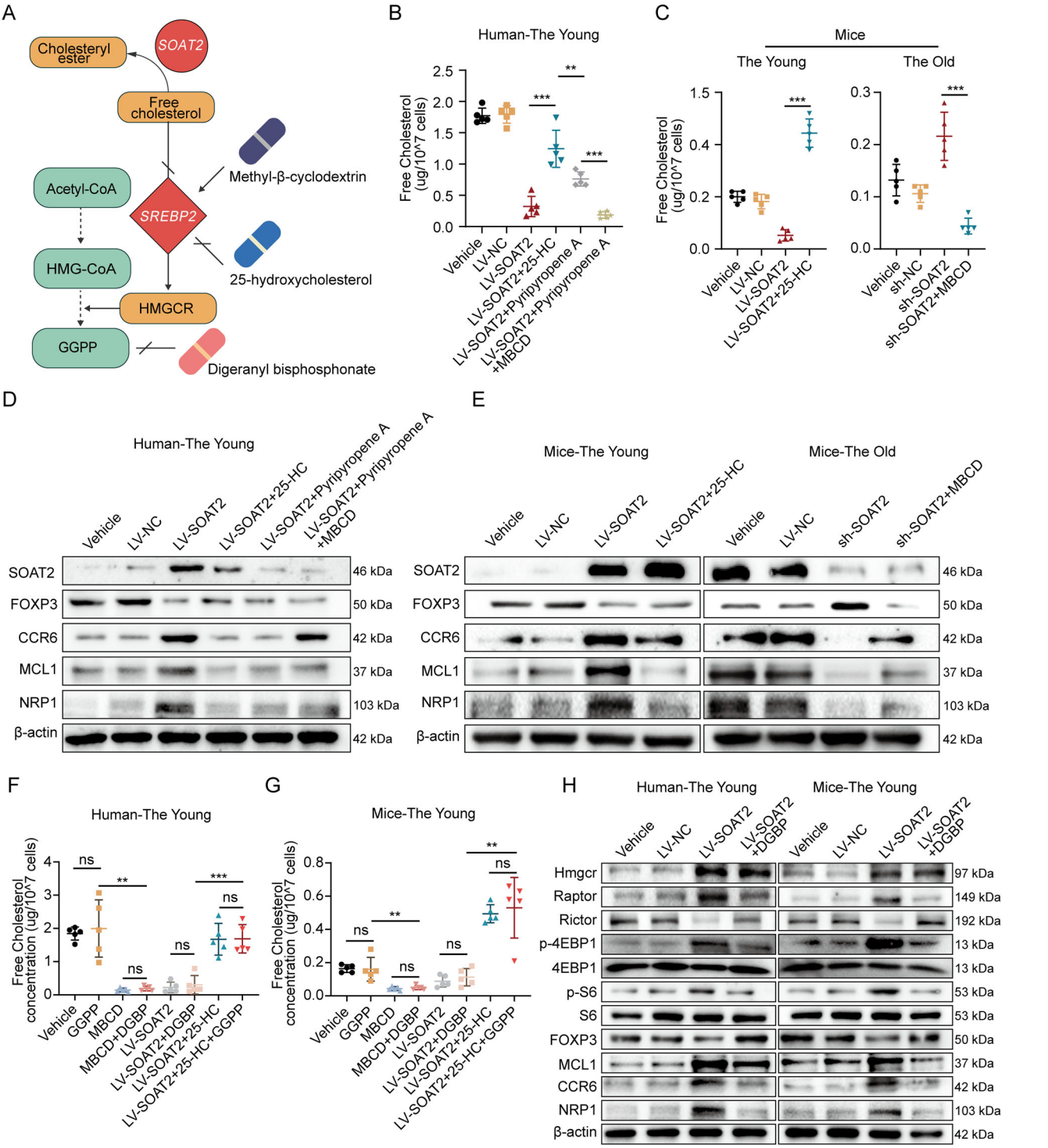


**Fig. 8 | SOAT2 promotes cholesterol metabolism in Treg cells by activating the SREBP2-HMGCR-GGPP pathway. A** Schematic representation of SOAT2 affects cholesterol metabolism through regulating SREBP2-HMGCR-GGPP pathway. **B**, **C** The content of free cholesterol components were measured by the Cholesterol Assay Kit in indicated groups ($n = 5$). **D**, **E** The proteins extracted from human or murine Treg cells in indicated groups were assessed by Western blotting analysis. The experiment was repeated 3 times independently with similar results. **F**, **G** The content of free cholesterol components were measured by the Cholesterol Assay Kit in indicated groups ($n = 5$). **H** The proteins extracted from human or murine Treg cells in indicated groups were assessed by Western blotting analysis. The experiment was repeated 3 times independently with similar results. Data represented means ± SD. Statistical difference was evaluated by one-way ANOVA test (**B**, **C**, **F**, **G**). Source data are provided as a Source Data file. (**$P < 0.01$; ***$P < 0.001$; ns no significance).

closely associated with physiological and metabolic shifts during aging and may impact health status and disease risk in elderly individuals. They affect cellular cholesterol homeostasis and lipid metabolism, leading to elevated SOAT2 expression. Variations in PUFA levels and cytochrome P450-related metabolites also modulate lipid metabolism pathways, indirectly enhancing SOAT2 expression. Furthermore, changes in inflammatory markers and complement proteins influence immune cell function and metabolism, resulting in compensatory increases in lipid-processing enzymes such as SOAT2[53].

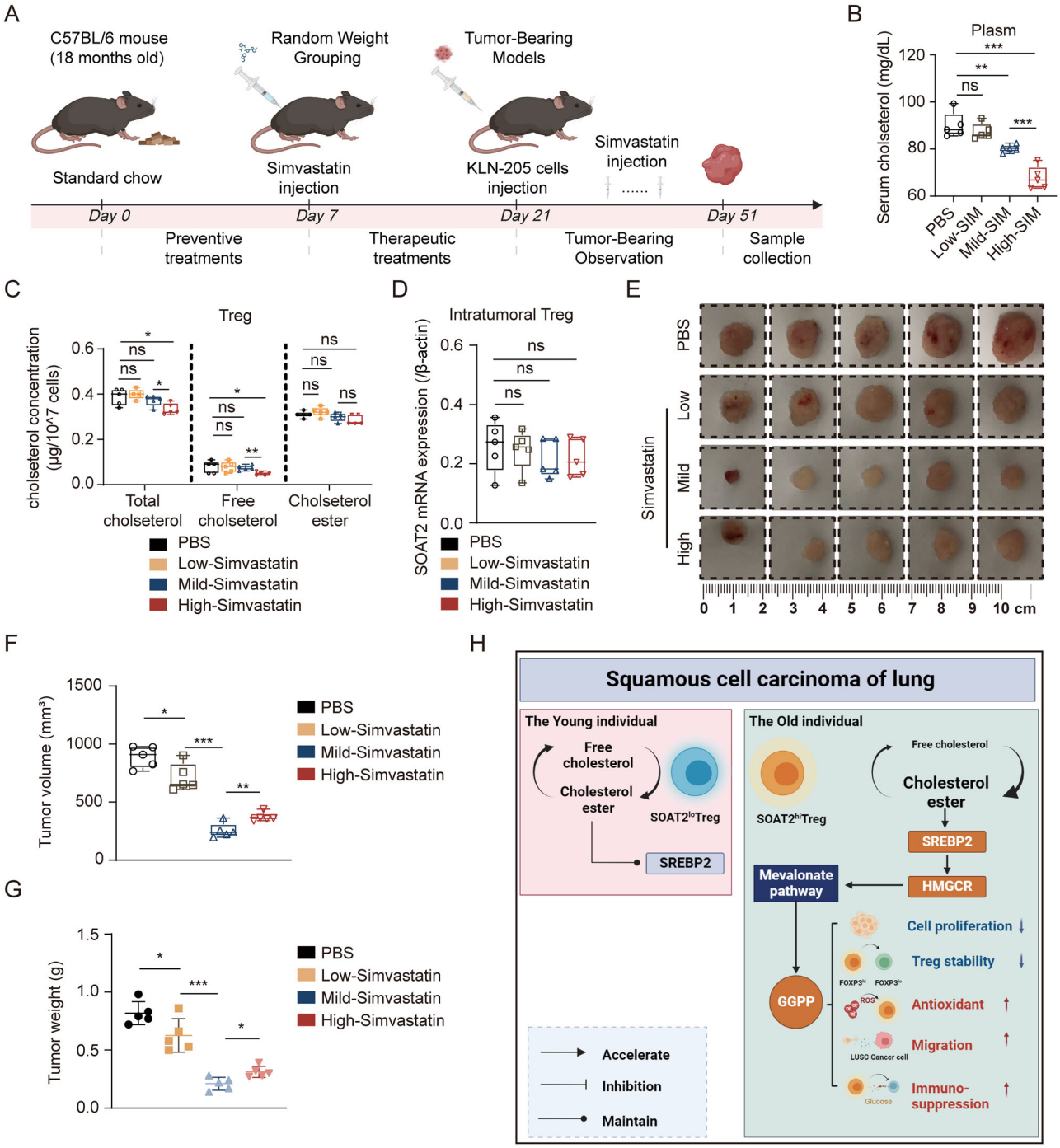


**Fig. 9 | Excessive suppression of cholesterol promotes tumor growth in elderly mice. A** Schematic design of the KLN-205 cells allograft model. Four groups: PBS, low-dose simvastatin (2.5 mg/kg), medium-dose simvastatin (25 mg/kg), and high-dose simvastatin (50 mg/kg) ($n = 5$) (Created in BioRender. Major, Z. (2024) https://BioRender.com/z47q423). **B** The content of plasm cholesterol components were measured by the Cholesterol Assay Kit in the four groups. **C** The content of total cholesterol, free cholesterol, and cholesterol ester components in the Tregs were measured by the Cholesterol Assay Kit in the four groups. **D** The mRNA expression of SOAT2 in the intratumoral Tregs was monitored by quantitative RT-PCR using gene-specific primers and probes. **E**–**G** Representative images of subcutaneous tumors (**E**), tumor volume (**F**), and tumor weight (**G**) in indicated groups. **H** The mechanism of SOAT2 exerts immunosuppression in elderly LSCC patients (Created in BioRender. Major, Z. (2022) https://BioRender.com/f54k103). Data represented means ± SD. Statistical difference was evaluated by one-way ANOVA test (**B**, **C**, **D**, **F**, **G**). Source data are provided as a Source Data file. (*$P < 0.05$; **$P < 0.01$; ***$P < 0.001$; ns no significance).

High-SOAT2 Tregs predominantly exert their immunosuppressive effects through competitive cholesterol uptake, which is manifested in several key aspects: (1) Maintenance of Treg Cell Membrane Integrity: High-SOAT2 Tregs enhance their suppression of Teffs through increased cholesterol absorption. Cholesterol is essential for maintaining the structural integrity of Tregs membranes and lipid rafts, which are essential for effective interaction with Teffs[54]. (2) Enhanced Metabolic Support: Elevated cholesterol metabolism supports the energy and metabolic demands of Tregs. By ensuring robust metabolic activity, high cholesterol levels facilitate the sustained immunosuppressive functions of Tregs over prolonged periods[55]. (3) Regulation of Cell-Cell Interactions: Cholesterol modulates the formation of immune synapses between Tregs and Teffs. Increased cholesterol metabolism can enhance the stability and efficiency of these interactions, resulting

in more effective suppression of Teffs[56]. (4) Metabolic Reprogramming: Cholesterol uptake drives metabolic reprogramming in Tregs, enhancing fatty acid oxidation (FAO) and mitochondrial function. This metabolic adaptation provides Tregs with enhanced survival and immunosuppressive capabilities, particularly in the tumor microenvironment[57]. (5) Cholesterol Metabolites: Oxidized cholesterol derivatives, such as oxysterols, can enhance the immunosuppressive functions of Tregs by modulating signaling pathways[58]. These metabolites may inhibit Teffs activation through the regulation of immune checkpoint molecules, such as CTLA-4 and PD-1. Our study showed that SOAT2 exerts immunosuppressive function by promoting cholesterol metabolism in Treg cells.

In summary, in this study, we included elderly LSCC patients from public databases and the First Affiliated Hospital of Nanjing Medical University. Through bioinformatics statistics and radiomic analysis, we found that SOAT2 involved in immune infiltration predicts poor prognosis in older LSCC populations. Both in vivo and in vitro experiments confirmed that SOAT2 is specifically overexpressed on Treg cells in elderly individuals, exerting an immunosuppressive effect and thereby promoting tumor progression. Mechanically, SOAT2 promotes cholesterol metabolism in Treg cells by activating the SREBP2-HMGCR-GGPP pathway, and then, induces Teffs cellular senescence via competitive cholesterol metabolism of Treg cells (Fig. 9H).

## Methods

### Public database and bioinformatics analysis

Lung Squamous Cell Carcinoma TCGA dataset were obtained from the UCSC Xena website (https://xenabrowser.net/datapages/). Immune and stromal scores were calculated by ESTIMATE algorithm. The differentially expressed genes (DEGs) were identified by R software (version 3.8.0) with package limma by LogFC statistical cutoff[59]. The OS-related genes were identified by the multivariable Cox proportional risk regression[60]. The abundance of immune infiltrates of DEGs in LSCC were analyzed by TIMER, including B cells, $CD4^+$ T cells, $CD8^+$ T cells, neutrophils, macrophages, and dendritic cells, as well as the tumor purity. SOAT2 associated biological mechanism and KEGG pathway enrichment were evaluated by Gene set enrichment analysis (GSEA, https://www.gsea-msigdb.org/gsea/index.jsp). SOAT2 associated protein-protein interaction (PPI) network was retrieved from STRING database(https://string-db.org/) and reconstructed using ClueGO by Cytoscape software[61,62]. Gene Ontology biological process (GO_BP), cell components (GO_CC) and molecular functions (GO_MF), KEGG pathway enrichment were also analyzed by the function module of ClueGO. The GTEx (https://www.gtexportal.org) and GEO database (https://www.ncbi.nlm.nih.gov) were used to evaluate the expression profile of SOAT2 in different tissues and ages.

### The radiomics analysis

Patients included in this radiomics analysis were obtained from the TCGA database (https://portal.gdc.cancer.gov/) and The Cancer Imaging Archive (TCIA) (https://www.cancerimagingarchive.net/). According to the following inclusion exclusion criteria, we collected a total of 176 patients, 33 from TCGA database and 143 from TCIA database. Inclusion criteria were (1) pathologic diagnosis of lung squamous cell carcinoma; (2) plain and contrast-enhanced CT radiomic of the chest with dual-source CT prior to chemoradiotherapy and other therapies; (3) over 65 years old; (4) complete clinical data. Exclusion criteria were (1) insufficient CT quality to obtain measurements; (2) less than 6 months of follow-up; (3) loss of follow up.

The training cohort (Fig. 2A): 143 Patients from the TCIA database were assigned to the training cohort. The dual-source computed tomography (CT) image files of the patient in the pre-treatment format of DICOM were downloaded from the TCIA database, including cross-sectional and coronal plane, and the files were imported into 3Dslicer 5.0.3 (https://www.slicer.org/) for analysis. Subsequently, three radiologists manually outlined the region of interest (ROI) using lung window and mediastinal window data understanding the clinical ending (excluding tumor borders and calcified, cystic, or necrotic regions). Intraclass correlation coefficient were used to assess the consistency of the three radiologists in outlining the target area ($C > 0.8$). A total of 1714 ROI features data include First-order statistics, Texture, gray-level co-occurrence matrix (GLCM), gray-level run length matrix (GLRLM), gray level size zone matrix (GLSZM), neighborhood gray-tone difference matrix (NGTDM), gray level dependence matrix (GLDM), Shape(3D/2D), Wavelet (LL/HHH, LHL/LLH, HLL/HLH, HHL/LHH) were extracted after quality control and standardization. Then, these features were classified using consensus unsupervised cluster analysis and $k = 3$ was obtained as the optimal classification. For further screening, Logistic regression and CLRM analysis were performed with prognostic time as the outcome measure and finally obtained three features: original_glszm_HighGrayLevelZoneEmphasis (gray-level size zone matrix feature), wavelet-HHH_glrlm_LongRunHighGrayLevelEmphasis (gray-level run-length matrix feature), and square_glszm_SizeZoneNonUniformityNormalized (gray-level size zone matrix feature).

The validation cohort (Fig. 2B): 33 Patients from the TCGA database were assigned to the validation cohort. Kaplan–Meier analysis was using to validate the three features in the radiomic risk model was correlated with the patient's OS, and the results were presented in the heat map. Then, we determined the optimal cutoff value to dichotomize patients into high-risk and low-risk subgroups. The prediction power of the model was evaluated using the receiver operating characteristic (ROC) analysis. Multivariate Cox regression analysis was conducted to evaluate whether the clinical features and risk score was independent of other radiomic features, including age, gender, grade and pathological stage. Risk models that combine clinical and radiomic features are presented in a nomogram and validated by ROC curves.

The LSCC patients over 65 years old from the First Affiliated Hospital of Nanjing Medical University in 2017 to 2019, excluding patients without preoperative imaging, histopathological testing, and missing follow-up. With the informed consent of the patients, 46 patients were incorporated into this study. The radiomic-clinical nomogram model and radiomic model were applied to 46 patients to derive the corresponding risk scores (Fig. 2A). This study was approved by the Ethics Committee of the First Affiliated Hospital of Nanjing Medical University (IACUC-2206030).

### Peripheral blood lymphocytes

The peripheral blood mononuclear cells (PBMC) fraction was isolated from peripheral blood by Ficoll-Paque density gradient separation using standard protocols and cryopreserved until later use.

### Cell culture

Mouse lung squamous carcinoma cells KLN-205 and human lung squamous carcinoma cells H226 were cultured in high-glucose DMEM. Media were supplemented with 10% FBS, 1% penicillin/streptomycin. All cells were maintained at 37 °C with 5% $CO_2$. Freeze-down stocks of the original characterized cell lines were cryopreserved in liquid nitrogen. All experiments were performed using cells with <10 passages in continuous culture.

### T Cell isolation, culture, and lentiviral transfection

Single-cell suspensions were extracted from mouse tumor tissues and splenic organ, and peripheral blood of healthy volunteers as previously reported[63]. For mouse samples, $CD4^+CD25^+FOXP3^+$ T lymphocyte cells (Treg cells), $CD4^-$ T lymphocyte cells, $CD8^+$ TILs (Teffs) were enriched and sorted from spleen and tumor tissues using a modified isolation protocol by Regulatory T Cell Isolation Kit and $CD8^+$ TILs Isolation Kit (#130-091-041, #130-116-478, Miltenyi Biotec). For human samples, single-cell suspensions from human peripheral blood were gathered

and extracted with $CD4^+CD25^+CD45RA^+$ Regulatory T Cell Isolation Kit (#130-093-631, Miltenyi Biotec) or $CD8^+CD45RA^+$ Effector T Cell Isolation Kit (#130-094-485, Miltenyi Biotec). Treg cells were cultured in TexMACS™ Medium (#130-097-196, Miltenyi Biotec) containing IL-2 (100 U/ml) (#Z02764, #Z03074, Genscript) and TGF-β (10 ng/ml) (#Z03431, #Z03411, Genscript). The Treg Expansion Kit (#130-095-345, #130-095-925, Miltenyi Biotec) was applied for Treg multiplication at a bead-to-cell ratio of 4:1 for human or 3:1 for mice, where recombinant interleukin 2 (rIL-2) with a concentration of 500 U/mL for human or 2000 U/mL for mice.

Human SOAT2 (NM_003578) overexpressing lentiviral vectors with GV643 vector, and lentiviruses for mouse SOAT2 (NM_146064) knockdown with GV644 vector or overexpression with GV655 vector were packaged according to the manufacturer's instruction from Genechem (Shanghai, China). Plasmids were as follows: GV643 vector: pRRLSIN-cPPT-SFFV-MCS-3FLAG-E2A-SV40-puromycin; GV644 vector: pRRLSIN-cPPT-U6-shRNA-SFFV-SV40-puromycin; GV655 vector: pRRLSIN-cPPT-SFFV-MCS-SV40-puromycin.

Viruses were purified using filter (0.45 um) and ultracentrifugation (25000 rpm, 105 min) steps and detected using a qPCR Lentivirus Titration Kit (Lenti-X, qRT-PCR Titration Kit, Takara). Treg cells were incubated with 1 mL of viral supernatant containing 1 μg/mL polybrene (#TR-1003, Sigma-Aldrich) in a 6-well plate. The plate was then spun at 1000 g and 32 °C at 4 h to facilitate viral infection. Following the spin-infection step, 1 mL of fresh medium was added to each well. To increase the transduction efficiency, the spin-infection step was repeated the next day with a fresh virus supernatant. In addition, 24 h after the second infection, cells were washed twice with PBS and resuspended in fresh medium with puromycin (0.1 ug/ml)[64]. Cells were then collected for subsequent assays. The quantitative RT-PCR was used to assay efficiency of SOAT2 knockdown or overexpression according to standard techniques[65].

## Animal models

The male C57BL/6 J mice were purchased from Gempharmatech (Nanjing, China; the stock# for mice strains: NO. T064543), and raised at Nanjing Medical University Experimental Animal Center (SPF level). All mice were housed in a pathogen-free facility under controlled conditions (26 °C, 40–70% humidity) with a 12-hour light/dark cycle. Sterile food and water were provided throughout the housing period. The experimental and control mice were co-housed. All mouse experiments were conducted according to local and international institutional guidelines and approved by the Animal Care Committee of Nanjing Medical University (IACUC-2105008, IACUC-2407095). End of the experiment, all mice were euthanized: The animals were placed in an IVC cage, with the $CO_2$ delivery line connected to the inlet of the water bottle. The $CO_2$ cylinder valve was opened, and the mice were monitored until they became motionless, ceased breathing, and exhibited pupil dilation. The $CO_2$ flow was then discontinued, and the mice were observed for an additional two minutes to confirm euthanasia. The Animal Care Committee of Nanjing Medical University requires that the tumor volume of mice should not exceed 2000$mm^3$ and the tumor weight should not exceed 10% of body weight. Nonetheless, in this study, the criterion for terminating the experiment was set as when the tumor volume of any mouse reached 1500 $mm^3$. Since this study pertains to subcutaneous tumor xenografting in aged mice, compared with young mice, these aged mice exhibit a relatively inferior tolerance to the physical burden induced by tumor growth. In light of offering appropriate end-of-life care for the aged mice, we thus adjusted the termination criterion of the experiment to 1500 $mm^3$.

The peripheral blood PBMC was extracted from 8-week-old or 24-month-old male C57BL/6 J mice, and tested SOAT2 expression through PCR analysis (IACUC-2105008). For constructing lung squamous carcinoma models in C57BL/6 J mice, KLN-205 cells were maintained in vitro, $10^6$ cells resuspended in 100 ul PBS and then injected subcutaneously in the right side of mouse back. The mice were grouped as follows: the high expression (i) or low expression (ii) of SOAT2 in the old mice (24-month-old), and the young mice (8-week-old) with low SOAT2 expression (iii). Tumor growth was monitored every five days until tumor-bearing mice were euthanized on day 75 post-inoculation, and tumor volumes and weights were measured from euthanized mice.

Cholesterol metabolism model (IACUC-2407095): 18-month-old male C57BL/6 mice were initially given a standard diet for one week, after which they were randomly assigned to four groups based on body weight: PBS, low-dose simvastatin (2.5 mg/kg), medium-dose simvastatin (25 mg/kg), and high-dose simvastatin (50 mg/kg). From the second week onward, the mice received oral gavage treatment according to their group assignments. On day 21, the mice were injected $10^7$ KLN-205 cells resuspended in 100 ul PBS subcutaneously in the right side of mouse back. The experiment was terminated on day 51, at which point tumor growth was evaluated.

## Immunohistochemistry

Paraffin-embedded tissue samples were sliced into 4 μm thick sections by paraffin slicer (HM340E, Thermo Fisher Scientific). Then, each slide was deparaffinized in 60 °C, followed by treatment with xylene and graded alcohol. After the antigen retrieval and being blocked with 5% bovine serum albumin, tissue slides were immunohistochemically stained by antibodies against Ki-67 (1:50, Proteintech, #27309-1-AP) and SOAT2 (1:20, Proteintech, #21852-1-AP), FOXP3 (1:100, Abcam, #ab215206), CD8 (1:50, Bioss, #bs-0648R), respectively. All of the staining was assessed by pathologists blinded to the origination of the samples and subject outcome. Then, hematoxylin was used for counterstaining, and morphologic images were observed with Olympus BX51 microscope.

## Quantitative real-time PCR

Total RNA extraction from primary human and mouse lymphocytes was performed using TRIzol reagent (Invitrogen), chloroform and isopropanol according to manufacturer's instructions. Triplicate real-time PCR reactions were performed in an ABI Prism 7500 (Agilent Technologies) using SYBR green PCR Master Mix (Life Technologies, Carlsbad, CA) according to manufacturer's protocol[66]. The mRNA levels were determined by using the $2-\Delta\Delta Ct$ method. The primers used were shown as Supplementary Table 1.

## Immunoblotting and antibodies

Cell samples were lysed with Lysis Buffer containing phosphatase and protease inhibitor cocktail (#P0013C, Beyotime) for 30 min to extract the total protein. Tissue samples were grinded into pieces with liquid nitrogen, and then lysed with enhanced Lysis Buffer (#P0013B, Beyotime) for 2 h to extract the total protein. A total of 40 ug of proteins from lysates were run on 10% SDS–PAGE and transferred to PVDF membrane (Millipore). Then, the PVDF membrane was blocked by 5% nonfat milk in TBST solution for 1 h at room temperature and incubated with the primary antibody overnight at 4 °C. After washing four times with PBST solution, the PVDF membrane was incubated with horseradish peroxidase (HRP)-conjugated secondary antibody for 1 h at room temperature. The antibodies used in the study were listed in the Supplementary Table 2. The intensity of each band was quantified using the ImageJ software (NIH, Bethesda, MD).

## Chemotaxis assay

Treg cells chemotaxis assays were performed using 24-well Transwell chemotaxis plates (3 um size pore, Corning)[67]. Culture supernatants from KLN-205 or H226 cells were added to the lower chamber of the Transwell plates, and Treg cells were added to the upper chamber. After 120 min at 37 °C, chemotaxis was quantified by detecting the numbers of cells that migrated into the lower chamber.

### In vitro differentiation assay

$CD4^+$ naive T cells were sorted from PBMCs of healthy young volunteers with the $CD4^+$ Naive T Cell Isolation Kit II (#130-094-131, Miltenyi Biotec) and single cell suspension of mouse spleen using the Naive $CD4^+$ T Cell Isolation Kit (#130-104-453, Miltenyi Biotec) according to the instruction manual. Naive $CD4^+$ T cells were then transfected as described in the Methods section of T Cell isolation, culture, and lentiviral transfection, and plated in flat-bottom plates at $5 \times 10^4$ cells/well and cultured for 5 days in the presence of plate-bound anti-CD3 (5 ug/ml), soluble anti-CD28 (10 ug/ml), IL2 (100 U/ml), rapamycin (2.5 mM), all-trans retinoic acid (0.25 mM)[68,69]. The induction efficiency of Treg cells was measured using flow cytometry by analyzing FOXP3 expression in $CD4^+$ $CD25^+$ T cells.

### Generation of tumor-reactive Teff cells

To increase the immunogenicity of tumor cells, $5 \times 10^6$ lung squamous carcinoma cells were resuspended in 8 mL of complete medium after treatment with IFN-γ, placed in a 75 $cm^2$ flask, and irradiated with 40 Gy using an Xray cabinet (RADSOURCE,160 kV/25 mA). After irradiation, cells were placed in a humidified incubator (5% $CO_2$, 37 °C) until used.

Whole peripheral blood lymphocytes were collected from young groups and placed in coculture with irradiated tumor cells at an effector to target (E:T) ratio of 5:1 for at least two weeks in the presence of 100 U/mL IL-2 and 20 ug/mL anti-PD-1-blocking antibody (#329902, Biolegend)[16]. Lung squamous carcinoma cells-specific $CD8^+$ T cells were isolated from the above mixture system using CD8 MicroBeads (#130-116-478, #130-045-201, Miltenyi Biotec)[70]. Tumor recognition by $CD8^+$ T cells was evaluated by staining for IFN-γ (#506504, #505806, BioLegend) and the degranulation marker CD107a (#328618, #121620, BioLegend), as well as the production of granzyme and perforin[16].

### Flow cytometry analysis

To detect lymphocyte proliferation, intracellular Ki67 was stained using a Cytofix/Cytoperm Kit (#554714, BD) followed by staining with Ki-67 antibody (#ab196907, Abcam). Then, cell proliferation rate was analyzed with the flow cytometer (Becton-Dickinson, San Jose, CA, USA). CFSE assay was carried out to detect the proliferation of cytotoxicity $CD8^+$ T cells that co-cultured with Treg cells as previously described[71]. In the coculture system, Teff cells were stained with 10 μM CFSE and seed in the lower well of the Transwell plate, where Treg cells cultured on 0.4 μm porous membrane inserts (Corning, NY, USA). The Teff-Treg cells were cultured at a 3:1 ratio (Teff: Treg) for 4 days, followed by flow cytometry.

For Lymphocyte apoptosis assay, the 7AAD and Annexin V apoptosis detection kit (#AP105, MultiSciences, China) was used for cell staining according to the manufacturer's instructions[72,73]. The functional phenotyping for surface markers of Teff cells was carried out using anti-CD27-PE (#124210) and anti-CD28-PE (#102106, #302940) from BioLegend (San Diego, USA).

The DNA double-strand breaks were detected by probing phosphorylated γ-H2AX (#613416, BioLegend) in Teff cells with Treg cells co-incubation. To determine the phenotype of the senescence lymphocyte fraction, Teff cells were harvested after specific treatment and stained with anti-CD45RA (Human, #983002, BioLegend, Mouse, #130-102-463, Miltenyibiotec) or anti-KLRG1(#138408, BioLegend). The exhaustion of lymphocytes was defined by surface markers of anti-TIM-3 (#11-5870-82, eBioscience) or anti-PD-1 (#329908, #135210, BioLegend) in Teff-cell populations with co-culture experiments.

Analyses of flow cytometry data were performed using Flow Jo software (version 9.6.2). All data were acquired using FACS Canto II and analyzed with the FlowJo software. All FACS sequential gating/sorting strategies are shown in the Supplementary Fig. 11 and 12.

### Cytokine measurement by ELISA

After restimulation with PMA (#HY-18739, MCE) + Ionomycin (#HY-13434, MCE) for 6 h, cytokine levels as following: IL-2 (#EK102HS, #EK202HS, MULTI SCIENCES), IL-10 (#EK110, #EK210, MULTI SCIENCES), IL-35 (#E-EL-H2443c, #E-EL-M0733c, Elabscience) and TGF-β (#EK981, MULTI SCIENCES) in Treg cells, was assessed by ELISA kits in the supernatants of the culture medium according to the product instruction. As well as Cytokine with ELISA kits was performed for assessment of IL-1β (#EK101B, EK201B, MULTI SCIENCES), IL-2 (#EK102HS, #EK202HS, MULTI SCIENCES), IL-4 (#EK104, #EK204, MULTI SCIENCES), IL-5 (#EK105, #EK205, MULTI SCIENCES), IL-6 (#EK106, SEKM-0046, Solarbio), IL-8 (Human, #EK108, MULTI SCIENCES, Mouse,), IL-10 (#EK110, #EK210, MULTI SCIENCES), IL-22 (#EK122, #EK222, MULTI SCIENCES), TNF-α (#EK182, #EK282, MULTI SCIENCES), TGF-β (#EK981, MULTI SCIENCES) and IFN-γ (#506504, #505806, BioLegend) from Teff cells. BioTek's Epoch2 Microplate Spectrophotometer (USA) determined OD values.

### ELISPOT assay

The treated teff cells produce cytokines, which are captured by specific monoclonal antibodies granzyme B (#674602, #662802, BioLegend) and perforin (#308102, #S16009A, BioLegend) on the PVDF membrane (pre-coated) at the bottom of the ELISPOT plate (#3654-TP-10, Mab-Tech). The captured cytokines granzyme B and perforin were labeled with biotin and then combined with horseradish peroxidase-labeled avidin. After adding substrate for staining, spots appeared on the PVDF membrane, and the spots were manually counted.

### LDH assay

Teff cells were co-cultured with Treg cells after lentivirus infection and collected for LDH assay as previously described[74]. The tumor cells were plated and stimulated with Teff cells in RPMI 1640. LDH assay was performed according to the manufacturer's instructions (#C0017, Beyotime). Relative LDH release from tumor cells was calculated as: LDH release [%] = 100 × (measurement − unstimulated control) / (lysis control − unstimulated control).

### Senescence-associated β-galactosidase staining

To analyse Treg cells-induced Teff senescence in vitro as report, a co-culture system with Treg cells and Teff was developed using β-Galactosidase Staining Kit (#C0602, Beyotime). Senescence associated β-galactosidase assays were performed as previously described[75]. The stained samples were viewed under an Olympus iX80 microscope with bright field illumination. The percentage of β-galactosidase positive undergoing senescence (stained green) were determined by counting the number of the green cells and normalising them to the total number of the cells in the same image.

### Cellular cholesterol measurement

The Cholesterol/Cholesterol Ester Quantitation Kit (#ab65359, Abcam) was used to determine the cellular concentrations of cholesterol and cholesteryl ester according to the manufacturer's instructions. Concentration of samples was calculated as:

Cholesterol Concentration = (Amount of cholesterol (μg) determined from Standard Curve) / (Volume of sample (μL) added into the reaction well.) × Dilution Factor.

### Statistical analysis

All statistical analyses were performed using R software and Bioconductor. The data were represented as the mean ± standard deviation. The difference between two groups was evaluated by two-tailed Student's $t$ test, whereas the difference among multiple groups was evaluated by one-way ANONA. $P < 0.05$ stood for significant difference (ns, no significance; $^*P$-value $< 0.05$; $^{**}P < 0.01$; $^{***}P < 0.001$).

### Reporting summary

Further information on research design is available in the Nature Portfolio Reporting Summary linked to this article.

## Data availability

All data are included in the Supplementary Information or available from the authors, as are unique reagents used in this Article. The raw numbers for charts and graphs are available in the Source Data file. Source data are provided with this paper.

## References


1. Sung, H. et al. Global cancer statistics 2020: GLOBOCAN estimates of incidence and mortality worldwide for 36 cancers in 185 countries. *CA Cancer J. Clin.* **71**, 209–249 (2021).
2. Siegel, R. L., Miller, K. D., Fuchs, H. E. & Jemal, A. Cancer statistics, 2022. *CA Cancer J. Clin.* **72**, 7–33 (2022).
3. Socinski, M. A. et al. Current and emergent therapy options for advanced squamous cell lung cancer. *J. Thorac. Oncol.* **13**, 165–183 (2018).
4. Burton, D. G. A. & Stolzing, A. Cellular senescence: immunosurveillance and future immunotherapy. *Ageing Res. Rev.* **43**, 17–25 (2018).
5. Lian, J., Yue, Y., Yu, W. & Zhang, Y. Immunosenescence: a key player in cancer development. *J. Hematol. Oncol.* **13**, 151 (2020).
6. Zhen, Z. et al. Nuclear cGAS restricts L1 retrotransposition by promoting TRIM41-mediated ORF2p ubiquitination and degradation. *Nat. Commun.* **14**, 8217 (2023).
7. Zabransky, D. J., Jaffee, E. M. & Weeraratna, A. T. Shared genetic and epigenetic changes link aging and cancer. *Trends Cell Biol.* **32**, 338–350 (2022).
8. Saleh, R. & Elkord, E. FoxP3(+) T regulatory cells in cancer: prognostic biomarkers and therapeutic targets. *Cancer Lett.* **490**, 174–185 (2020).
9. Xu, T. et al. Metabolic control of T(H)17 and induced T(reg) cell balance by an epigenetic mechanism. *Nature* **548**, 228–233 (2017).
10. Zeng, H. et al. mTORC1 couples immune signals and metabolic programming to establish T(reg)-cell function. *Nature* **499**, 485–490 (2013).
11. Schmidt, N. M. et al. Targeting human Acyl-CoA:cholesterol acyltransferase as a dual viral and T cell metabolic checkpoint. *Nat. Commun.* **12**, 2814 (2021).
12. Galgani, M., De Rosa, V., La Cava, A. & Matarese, G. Role of metabolism in the immunobiology of regulatory T cells. *J. Immunol.* **197**, 2567–2575 (2016).
13. Togashi, Y., Shitara, K. & Nishikawa, H. Regulatory T cells in cancer immunosuppression - implications for anticancer therapy. *Nat. Rev. Clin. Oncol.* **16**, 356–371 (2019).
14. Kang, J. H. & Zappasodi, R. Modulating Treg stability to improve cancer immunotherapy. *Trends Cancer* **9**, 911–927 (2023).
15. Verma, A. et al. T-regulatory cells in tumor progression and therapy. *Cancer Manag. Res.* **11**, 10731–10747 (2019).
16. Dijkstra, K. K. et al. Generation of tumor-reactive T cells by co-culture of peripheral blood lymphocytes and tumor organoids. *Cell* **174**, 1586–1598.e1512 (2018).
17. Blair, A. B. et al. IDO1 inhibition potentiates vaccine-induced immunity against pancreatic adenocarcinoma. *J. Clin. Invest.* **129**, 1742–1755 (2019).
18. Mohile, S. G. et al. Communication with older patients with cancer using geriatric assessment: a cluster-randomized clinical trial from the national cancer institute community oncology research program. *JAMA Oncol.* **6**, 196–204 (2020).
19. Chow, A., Perica, K., Klebanoff, C. A. & Wolchok, J. D. Clinical implications of T cell exhaustion for cancer immunotherapy. *Nat. Rev. Clin. Oncol.* **19**, 775–790 (2022).
20. Liu, X., Hoft, D. F. & Peng, G. Senescent T cells within suppressive tumor microenvironments: emerging target for tumor immunotherapy. *J. Clin. Invest.* **130**, 1073–1083 (2020).
21. Liu, X. et al. Regulatory T cells trigger effector T cell DNA damage and senescence caused by metabolic competition. *Nat. Commun.* **9**, 249 (2018).
22. Lim, S. A. et al. Lipid signalling enforces functional specialization of T(reg) cells in tumours. *Nature* **591**, 306–311 (2021).
23. Willett, K. M., Gillett, N. P., Jones, P. D. & Thorne, P. W. Attribution of observed surface humidity changes to human influence. *Nature* **449**, 710–712 (2007).
24. Zhang, Y. et al. The role of KLRG1: a novel biomarker and new therapeutic target. *Cell Commun. Signal* **22**, 337 (2024).
25. Martins, R. et al. Disease tolerance as an inherent component of immunity. *Annu. Rev. Immunol.* **37**, 405–437 (2019).
26. Duvel, K. et al. Activation of a metabolic gene regulatory network downstream of mTOR complex 1. *Mol. Cell* **39**, 171–183 (2010).
27. Valbuena Perez, J. V. et al. Altered glucocorticoid metabolism represents a feature of macroph-aging. *Aging Cell* **19**, e13156 (2020).
28. Deleidi, M. & Rubino, JaggleM. G. Immune aging, dysmetabolism, and inflammation in neurological diseases. *Front. Neurosci.* **9**, 172 (2015).
29. Fane, M. & Weeraratna, A. T. How the ageing microenvironment influences tumour progression. *Nat. Rev. Cancer* **20**, 89–106 (2020).
30. DeSantis, C. E. et al. Cancer statistics for adults aged 85 years and older, 2019. *CA Cancer J. Clin.* **69**, 452–467 (2019).
31. Bottazzi, B., Riboli, E. & Mantovani, A. Aging, inflammation and cancer. *Semin Immunol.* **40**, 74–82 (2018).
32. Nikolich-Zugich, J. The twilight of immunity: emerging concepts in aging of the immune system. *Nat. Immunol.* **19**, 10–19 (2018).
33. Goronzy, J. J. & Weyand, C. M. Successful and maladaptive T cell aging. *Immunity* **46**, 364–378 (2017).
34. Goronzy, J. J. & Weyand, C. M. Mechanisms underlying T cell ageing. *Nat. Rev. Immunol.* **19**, 573–583 (2019).
35. Raynor, J. et al. IL-6 and ICOS antagonize bim and promote regulatory T cell accrual with age. *J. Immunol.* **195**, 944–952 (2015).
36. Chougnet, C. A. et al. A major role for Bim in regulatory T cell homeostasis. *J. Immunol.* **186**, 156–163 (2011).
37. Darrigues, J., van Meerwijk, J. P. M. & Romagnoli, P. Age-dependent changes in regulatory T lymphocyte development and function: a mini-review. *Gerontology* **64**, 28–35 (2018).
38. Cluxton, D., Petrasca, A., Moran, B. & Fletcher, J. M. Differential regulation of human treg and Th17 cells by fatty acid synthesis and glycolysis. *Front. Immunol.* **10**, 115 (2019).
39. Vaeth, M. et al. Tissue resident and follicular Treg cell differentiation is regulated by CRAC channels. *Nat. Commun.* **10**, 1183 (2019).
40. Shi, H. & Chi, H. Metabolic control of treg cell stability, plasticity, and tissue-specific heterogeneity. *Front. Immunol.* **10**, 2716 (2019).
41. Fung, I. T. H. et al. Activation of group 2 innate lymphoid cells alleviates aging-associated cognitive decline. *J. Exp. Med.* **217**, e20190915 (2020).
42. Yang, W. et al. Potentiating the antitumour response of CD8(+) T cells by modulating cholesterol metabolism. *Nature* **531**, 651–655 (2016).
43. Hao, M. et al. Combination of metabolic intervention and T cell therapy enhances solid tumor immunotherapy. *Sci. Transl. Med.* **12**, eaaz6667 (2020).
44. Pan, J. et al. Potentiation of Kras peptide cancer vaccine by avasimibe, a cholesterol modulator. *EBioMedicine* **49**, 72–81 (2019).
45. Liu, X. et al. Reprogramming lipid metabolism prevents effector T cell senescence and enhances tumor immunotherapy. *Sci. Transl. Med.* **13**, eaaz6314 (2021).

46. Warrier, M. et al. Sterol O-acyltransferase 2-driven cholesterol esterification opposes liver X receptor-stimulated fecal neutral sterol loss. *Lipids* **51**, 151–157 (2016).
47. Parini, P. et al. ACAT2 is localized to hepatocytes and is the major cholesterol-esterifying enzyme in human liver. *Circulation* **110**, 2017–2023 (2004).
48. Min, H. K. et al. Increased hepatic synthesis and dysregulation of cholesterol metabolism is associated with the severity of nonalcoholic fatty liver disease. *Cell Metab.* **15**, 665–674 (2012).
49. Nguyen H. T. L., Kasapis S., Mantri N. Physicochemical properties and effects of honeys on key biomarkers of oxidative stress and cholesterol homeostasis in HepG2 Cells. *Nutrients* **13**, 151 (2021).
50. Yeganeh, B. et al. Targeting the mevalonate cascade as a new therapeutic approach in heart disease, cancer and pulmonary disease. *Pharm. Ther.* **143**, 87–110 (2014).
51. Timilshina, M. et al. Activation of mevalonate pathway via LKB1 is essential for stability of T(reg) cells. *Cell Rep.* **27**, 2948–2961.e2947 (2019).
52. Prado, D. S. et al. Pitavastatin ameliorates autoimmune neuroinflammation by regulating the Treg/Th17 cell balance through inhibition of mevalonate metabolism. *Int. Immunopharmacol.* **91**, 107278 (2021).
53. Panyard, D. J., Yu, B. & Snyder, M. P. The metabolomics of human aging: advances, challenges, and opportunities. *Sci. Adv.* **8**, eadd6155 (2022).
54. Nazarov-Stoica, C., Surls, J., Bona, C., Casares, S. & Brumeanu, T. D. CD28 signaling in T regulatory precursors requires p56lck and rafts integrity to stabilize the Foxp3 message. *J. Immunol.* **182**, 102–110 (2009).
55. Chen, H. M. et al. Blocking immunoinhibitory receptor LILRB2 reprograms tumor-associated myeloid cells and promotes antitumor immunity. *J. Clin. Invest.* **128**, 5647–5662 (2018).
56. Ikenouchi J., Shigetomi K. Role of lipids in the organization of tight junction. *Microscopy* **73**, 457–462 (2024).
57. Cai, F., Jin, S. & Chen, G. The effect of lipid metabolism on CD4(+) T cells. *Mediators Inflamm.* **2021**, 6634532 (2021).
58. Wang, T. et al. 27-hydroxycholesterol causes cognitive deficits by disturbing Th17/Treg balance and the related immune responses in mild cognitive impairment patients and C57BL/6J mice. *J. Neuroinflamm.* **20**, 305 (2023).
59. Ritchie, M. E. et al. limma powers differential expression analyses for RNA-sequencing and microarray studies. *Nucleic Acids Res.* **43**, e47 (2015).
60. Friedman, J., Hastie, T. & Tibshirani, R. Regularization paths for generalized linear models via coordinate descent. *J. Stat. Softw.* **33**, 1–22 (2010).
61. Szklarczyk, D. et al. STRING v10: protein-protein interaction networks, integrated over the tree of life. *Nucleic Acids Res.* **43**, D447–D452 (2015).
62. Bindea, G. et al. ClueGO: a Cytoscape plug-in to decipher functionally grouped gene ontology and pathway annotation networks. *Bioinformatics* **25**, 1091–1093 (2009).
63. Wang, W. et al. Effector T cells abrogate stroma-mediated chemoresistance in ovarian cancer. *Cell* **165**, 1092–1105 (2016).
64. Lee, J., Sadelain, M. & Brentjens, R. Retroviral transduction of murine primary T lymphocytes. *Methods Mol. Biol.* **506**, 83–96 (2009).
65. Kennedy, A. & Cribbs, A. P. Production and concentration of lentivirus for transduction of primary human T cells. *Methods Mol. Biol.* **1448**, 85–93 (2016).
66. Tang, D. et al. Dietary restriction improves repopulation but impairs lymphoid differentiation capacity of hematopoietic stem cells in early aging. *J. Exp. Med* **213**, 535–553 (2016).
67. Peng, G. et al. Tumor-infiltrating gammadelta T cells suppress T and dendritic cell function via mechanisms controlled by a unique toll-like receptor signaling pathway. *Immunity* **27**, 334–348 (2007).
68. Meller, S. et al. T(H)17 cells promote microbial killing and innate immune sensing of DNA via interleukin 26. *Nat. Immunol.* **16**, 970–979 (2015).
69. Schmidt A., Elias S., Joshi R. N., Tegner J. In vitro differentiation of human CD4+FOXP3+ induced regulatory T cells (iTregs) from Naive CD4+ T cells using a TGF-beta-containing protocol. *J. Vis. Exp.* **118**, 55015 (2016).
70. Jie, X. et al. Targeting KDM4C enhances CD8(+) T cell mediated antitumor immunity by activating chemokine CXCL10 transcription in lung cancer. *J. Immunother. Cancer* **10**, e003716 (2022).
71. Zhong, X. P. et al. Enhanced T cell responses due to diacylglycerol kinase zeta deficiency. *Nat. Immunol.* **4**, 882–890 (2003).
72. Li, P. et al. Glutathione peroxidase 4-regulated neutrophil ferroptosis induces systemic autoimmunity. *Nat. Immunol.* **22**, 1107–1117 (2021).
73. Yamamoto, Y. et al. Surface phenotype changes and increased response to oxidative stress in CD4(+)CD25(high) T cells. *Biomedicines* **9**, 616 (2021).
74. Jain, P. et al. Characteristics, outcomes, prognostic factors and treatment of patients with T-cell prolymphocytic leukemia (T-PLL). *Ann. Oncol.* **28**, 1554–1559 (2017).
75. Dimri, G. P. et al. A biomarker that identifies senescent human cells in culture and in aging skin in vivo. *Proc. Natl Acad. Sci. USA* **92**, 9363–9367 (1995).


## Acknowledgements

We thank the volunteers and LSCC patients who made this study possible by donating their clinical samples. We also thank the first clinical medical college of Nanjing Medical University for providing technical assistance. This work was supported by the National Natural Science Foundation of China (No. 82171576 to J.W., and No. 82203771 to J.C.), the Province Capability Improvement Project through Science, Technology and Education (No. CXZX202228 to J.W.), the Jiangsu Leadership Health Management Research Project (No. BJ23004 to S.W., and No. BJ21027 to F.Z.), Natural Science Foundation of Jiangsu Higher Education Institutions (No.23KJA320004 to S.W.).

## Author contributions

M.Z., J.C., H.C. and Y.C.: writing–original draft, methodology, investigation, data curation, visualization. Q.C., F.Z., X.L., L.Q., Y.H. and X.K.: investigation, data curation. Y.Z.: supervision. S.W., J.W. and M.C.: writing–review & editing, project administration, resources, funding acquisition, conceptualization, methodology.

## Competing interests

The authors declare no competing interests.

## Additional information

**Supplementary information** The online version contains supplementary material available at https://doi.org/10.1038/s41467-025-56002-w.

**Correspondence** and requests for materials should be addressed to Minjie Chu, Shuangshuang Wu or Jianqing Wu.

**Peer review information** *Nature Communications* thanks Giorgia Cioccoloni, Eva Martínez-Cáceres who co-reviewed with Federico Fondelli and the other anonymous reviewer(s) for their contribution to the peer review of this work. A peer review file is available.